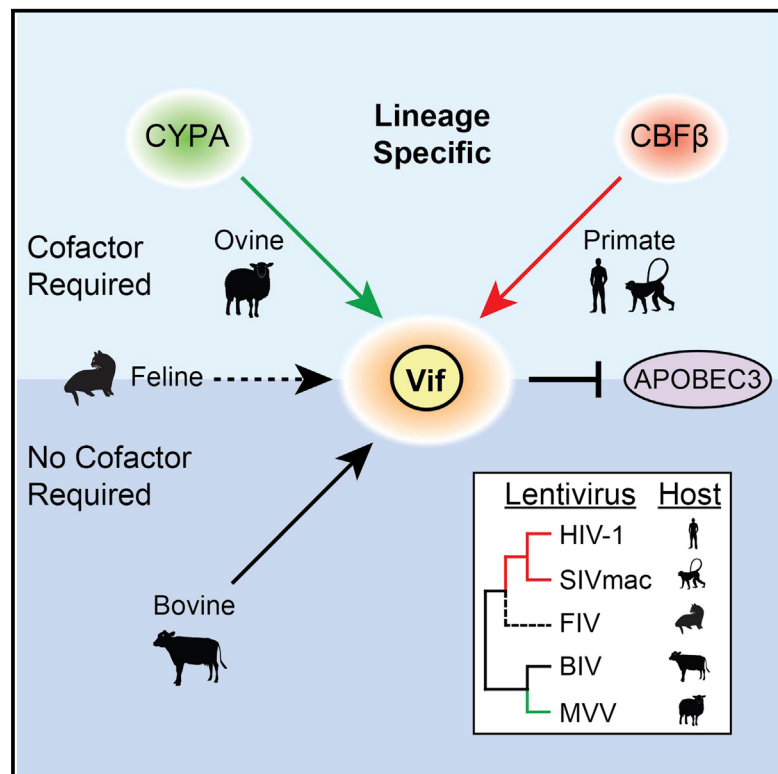


Lineage-Specific Viral Hijacking of Non-canonical E3 Ubiquitin Ligase Cofactors in the Evolution of Vif Anti-APOBEC3 Activity

Graphical Abstract



Authors

Joshua R. Kane, David J. Stanley, ..., John D. Gross, Nevan J. Krogan

Correspondence

john.gross@ucsf.edu (J.D.G.), nevan.krogan@ucsf.edu (N.J.K.)

In Brief

How viral proteins evolve functions without compromising ancestral ones is not well understood. Kane et al. now report that the lentiviral protein Vif has evolved to hijack host factors in a lineage-specific manner while conserving an ancestral viral-host complex promoting viral infection.

Highlights

- We present a comparative proteomic study of the viral protein Vif across the *Lentivirus* genus
- Only primate lentiviral Vif proteins require cofactor CBFβ
- BIV Vif requires no cofactor; MVV Vif requires a different cofactor, CYPA
- Cofactor use by Vif may serve as a gain-of-function mechanism

Lineage-Specific Viral Hijacking of Non-canonical E3 Ubiquitin Ligase Cofactors in the Evolution of Vif Anti-APOBEC3 Activity

Joshua R. Kane,^{1,2,5} David J. Stanley,³ Judd F. Hultquist,^{1,2,4,5} Jeffrey R. Johnson,^{1,2,5} Nicole Mietrach,⁶ Jennifer M. Binning,³ Stefán R. Jónsson,⁶ Sarah Barelier,³ Billy W. Newton,^{1,2,5} Tasha L. Johnson,^{1,2,5} Kathleen E. Franks-Skiba,^{1,2} Ming Li,⁴ William L. Brown,⁴ Hörður I. Gunnarsson,⁶ Adalbjorg Adalbjornsdóttir,⁶ James S. Fraser,^{2,7} Reuben S. Harris,⁴ Valgerður Andrésdóttir,⁶ John D. Gross,^{3,*} and Nevan J. Krogan^{1,2,5,*}

¹Department of Cellular and Molecular Pharmacology, University of California, San Francisco, San Francisco, CA 94158, USA

²California Institute for Quantitative Biosciences, QB3, University of California, San Francisco, San Francisco, CA 94158, USA

³Department of Pharmaceutical Chemistry, University of California, San Francisco, San Francisco, CA 94158, USA

⁴Department of Biochemistry, Molecular Biology and Biophysics, Institute for Molecular Virology, University of Minnesota, Minneapolis, MN 55455, USA

⁵J. David Gladstone Institutes, San Francisco, CA 94158, USA

⁶Institute for Experimental Pathology, University of Iceland, Keldur, 112 Reykjavík, Iceland

⁷Department of Bioengineering and Therapeutic Sciences, University of California, San Francisco, San Francisco, CA 94158, USA

*Correspondence: john.gross@ucsf.edu (J.D.G.), nevan.krogan@ucsf.edu (N.J.K.)

<http://dx.doi.org/10.1016/j.celrep.2015.04.038>

This is an open access article under the CC BY license (<http://creativecommons.org/licenses/by/4.0/>).

SUMMARY

HIV-1 encodes the accessory protein Vif, which hijacks a host Cullin-RING ubiquitin ligase (CRL) complex as well as the non-canonical cofactor CBF β , to antagonize APOBEC3 antiviral proteins. Non-canonical cofactor recruitment to CRL complexes by viral factors, to date, has only been attributed to HIV-1 Vif. To further study this phenomenon, we employed a comparative approach combining proteomic, biochemical, structural, and virological techniques to investigate Vif complexes across the lentivirus genus, including primate (HIV-1 and simian immunodeficiency virus macaque [SIVmac]) and non-primate (FIV, BIV, and MVV) viruses. We find that CBF β is completely dispensable for the activity of non-primate lentiviral Vif proteins. Furthermore, we find that BIV Vif requires no cofactor and that MVV Vif requires a novel cofactor, cyclophilin A (CYPA), for stable CRL complex formation and anti-APOBEC3 activity. We propose modular conservation of Vif complexes allows for potential exaptation of functions through the acquisition of non-CRL-associated host cofactors while preserving anti-APOBEC3 activity.

INTRODUCTION

Viruses must overcome host challenges to replicate successfully in an infected host. These challenges include not only the mechanics of viral entry, genome replication, assembly, and budding but also a variety of host-defined replication barriers,

both innate and adaptive. During productive infection, viral proteins rewire the host cell through a series of protein-protein interactions (PPIs) to promote viral replication. Systematic and unbiased mapping of these host-pathogen interactions can yield novel information concerning both viral biology and the endogenous functions of hijacked host factors.

An effective method for mapping host-pathogen interactions involves affinity purification of epitope-tagged viral proteins from host cells followed by mass spectrometry (AP-MS) to identify interacting host factors. This approach has been used to map global host-pathogen PPIs for HIV-1 (Jäger et al., 2012a), herpes (Davis et al., 2015), and hepatitis C (Ramage et al., 2015), as well as to study the PPIs of individual viral proteins in HPV (Tan et al., 2012; White et al., 2012a, 2012b), influenza (York et al., 2014), and picornaviruses (Greninger et al., 2012). Historically, these types of proteomic analyses have focused on a single virus or closely related sets of viruses and typically from the same (human) host.

In this study, we devised a strategy for the systematic, comparative analysis of host-pathogen PPIs focusing on the well-characterized lentivirus genus to analyze the complexes formed by representative Vif proteins from different lentiviral clades, including that of HIV-1. HIV-1 Vif is required for pathogenesis *in vivo* and serves as the virus' defense against host antiviral APOBEC3 (A3) proteins. In the absence of Vif, members of the A3 family of restriction factors package into budding virions, where they interfere with reverse transcription and induce lethal G-to-A hypermutation in viral cDNA (Harris et al., 2003; Iwatani et al., 2007; Mangeat et al., 2003; Zhang et al., 2003). HIV-1 Vif overcomes this replication block by acting as an adaptor between the A3 proteins and an endogenous ubiquitin ligase complex that catalyzes poly-ubiquitylation of the A3 proteins, resulting in their subsequent proteasomal degradation (Hultquist et al., 2011; Sheehy et al., 2002, 2003; Yu et al., 2003).

The HIV-1 Vif E3 ligase complex is composed of the endogenous CRL5 members, including Cullin-5 (CUL5), elongin B (ELOB), elongin C (ELOC), and RING-box protein 2 (RBX2), but also requires the additional Vif-dependent recruitment of a non-canonical cofactor, core-binding factor, beta subunit (CBF β) (Guo et al., 2014; Jäger et al., 2012b; Zhang et al., 2012). CBF β heterodimerizes with members of the RUNX family of transcription factors, serving to both stabilize RUNX steady-state levels and to enhance DNA-binding affinity (Huang et al., 2001; Tahirov et al., 2001). Recruitment of CBF β serves to stabilize HIV-1 Vif and is required for HIV-1 Vif A3 degradation activity in vivo (Hultquist et al., 2012; Jäger et al., 2012b; Kim et al., 2013; Miyagi et al., 2014; Zhang et al., 2012). Recent work has shown that this recruitment alters endogenous RUNX activity through competitive binding of HIV-1 Vif to CBF β , potentially to the benefit of the virus (Kim et al., 2013; Klase et al., 2014).

We chose to focus our comparative study on Vif for three primary reasons. First, a Vif protein is expressed in four of the five major lentiviral clades, each of which is known to mediate the proteasomal degradation of the cognate host A3 proteins (Larue et al., 2010). Second, unlike ubiquitously conserved lentiviral components such as Gag or Pol, Vif is not known to be required for the mechanics of viral replication and thus is potentially less constrained over the course of virus evolution. Third, whereas the mechanism of HIV-1 Vif-mediated A3 degradation is well characterized, little is known about the requirements for Vif proteins from other clades. Whereas recruitment of ELOC is assumed based on the conserved BC-box motif, it is unknown whether these Vif proteins recruit the same core E3 ligase complex and whether they require recruitment of a non-canonical E3 ligase component such as CBF β . In fact, recent work has suggested that other factors may be required for Vif stability and function in non-primate lentiviruses (Ai et al., 2014; Zhang et al., 2014a, b).

Here, we report a comparative proteomics strategy for the study of orthologous host-pathogen PPIs, which we subsequently use to analyze the complexes formed by representative Vif proteins from different lentiviral clades, including primate lentiviruses (HIV-1 and simian immunodeficiency virus macaque [SIVmac]), bovine immunodeficiency virus (BIV), feline immunodeficiency virus (FIV), and the ovine-tropic maedi-visna virus (MVV). We find that, whereas all lentiviral Vif orthologs can hijack the CRL5 complex in human cells, only primate lentiviral Vif proteins hijack CBF β and require it for A3 degradation. Whereas one non-primate lentiviral Vif, from BIV, appears to operate independently of any non-canonical cofactors, another Vif, from MVV, requires a novel non-canonical cofactor, cyclophilin A (CYPA), for in vitro reconstitution and in vivo A3-degrading activity. These results demonstrate an unexpected mechanistic flexibility in viral rewiring of the host cell despite the maintenance of a conserved activity. They furthermore suggest a modular conservation of host-pathogen interactions whereby novel PPIs may be formed with novel partners to serve the same functional purpose yet with potentially new orthogonal roles. We predict that the use of modular conservation to allow for mechanistic flexibility may be a generalizable model for viral protein evolution.

RESULTS

Divergent Vif Proteins Interact with a Conserved Host CRL Complex

All known lentiviruses express a Vif protein except for equine infectious anemia virus and the extinct rabbit endogenous lentivirus RELIK (Katzourakis et al., 2007; Kawakami et al., 1987). The Vif protein from each lentivirus is known to perform at least one conserved function, degradation of the restrictive A3 proteins from the cognate host (Hultquist et al., 2011; Larue et al., 2010; Sheehy et al., 2003; Yu et al., 2003). Despite this conservation in function, the primary sequence of these proteins is highly divergent, sharing no more than 25% identity of alignable residues between any pair (Figures 1A and S1A). The only obvious conserved motif is the ELOC-binding BC-box, which is known to be essential for A3 degradation. This has led to the hypothesis that each Vif protein mediates A3 degradation by recruitment of the same CRL5 complex, but a systematic characterization of each lentivirus' Vif complex had not previously been carried out.

In order to determine which host factors are physically bound to Vif proteins across the lentivirus phylogeny, we employed an unbiased proteomic approach using AP-MS to study five divergent Vif proteins from MVV, BIV, FIV, SIVmac, and HIV-1 (Table S1). Affinity tags comprising 2 \times Strep or 3 \times Flag were fused to either the amino (N) or carboxy (C) terminus of the Vif proteins, and tagged Vif constructs were either transiently expressed in HEK293T cells or used to make stable, doxycycline-inducible Jurkat T cell lines (Figure 1B). Tagged Vif proteins were affinity purified and eluates subjected to SDS-PAGE and silver staining (Figure 1C) and then analyzed by liquid chromatography coupled with tandem mass spectrometry (LC-MS/MS) to identify co-purified host factors (Jäger et al., 2012a). Putative interactions identified by AP-MS were scored using the significance analysis of interactome (SAINT) algorithm (Choi et al., 2011), and interactions with a SAINT probability score ≥ 0.9 in at least one Vif data set were included (Table S2). Prey scores were then organized by cell line and hierarchically clustered by correlation (Figure S2A). Within this data set, we observe expected interactions with CRL complex proteins, including CUL2, CUL5, ELOB, ELOC, RBX2, and RBX1, strongly suggesting a generally conserved mechanism for A3 proteasomal degradation among Vif proteins (Figure 1D). We observe within the data set a terminus-specific effect on Vif-CULLIN specificity between CUL2 and CUL5, particularly with the non-primate lentivirus Vif proteins (Figures 1D, 1E, and S2B–S2D).

The association of Vif with CBF β was only observed for primate lentivirus Vif proteins (SIVmac and HIV-1) in the AP-MS data sets for both HEK293T cells and Jurkat T cells (Figure 1D), an observation confirmed by immunoblot analysis (Figures 1E and S2B). To test whether Vif proteins not observed to physically interact with CBF β were still functionally regulated by the factor, we employed a single-cycle HIV-1 infectivity assay testing for Vif-mediated A3 degradation in the presence and absence of CBF β (Figure 2A). We observed that HIV-1 and SIVmac require CBF β for Vif-mediated rescue of HIV-1 infectivity from A3 restriction (Figures 2B and 2C), as previously reported (Hultquist et al., 2012; Jäger et al., 2012b). Conversely and consistent with the AP-MS results, the non-primate lentivirus Vif proteins

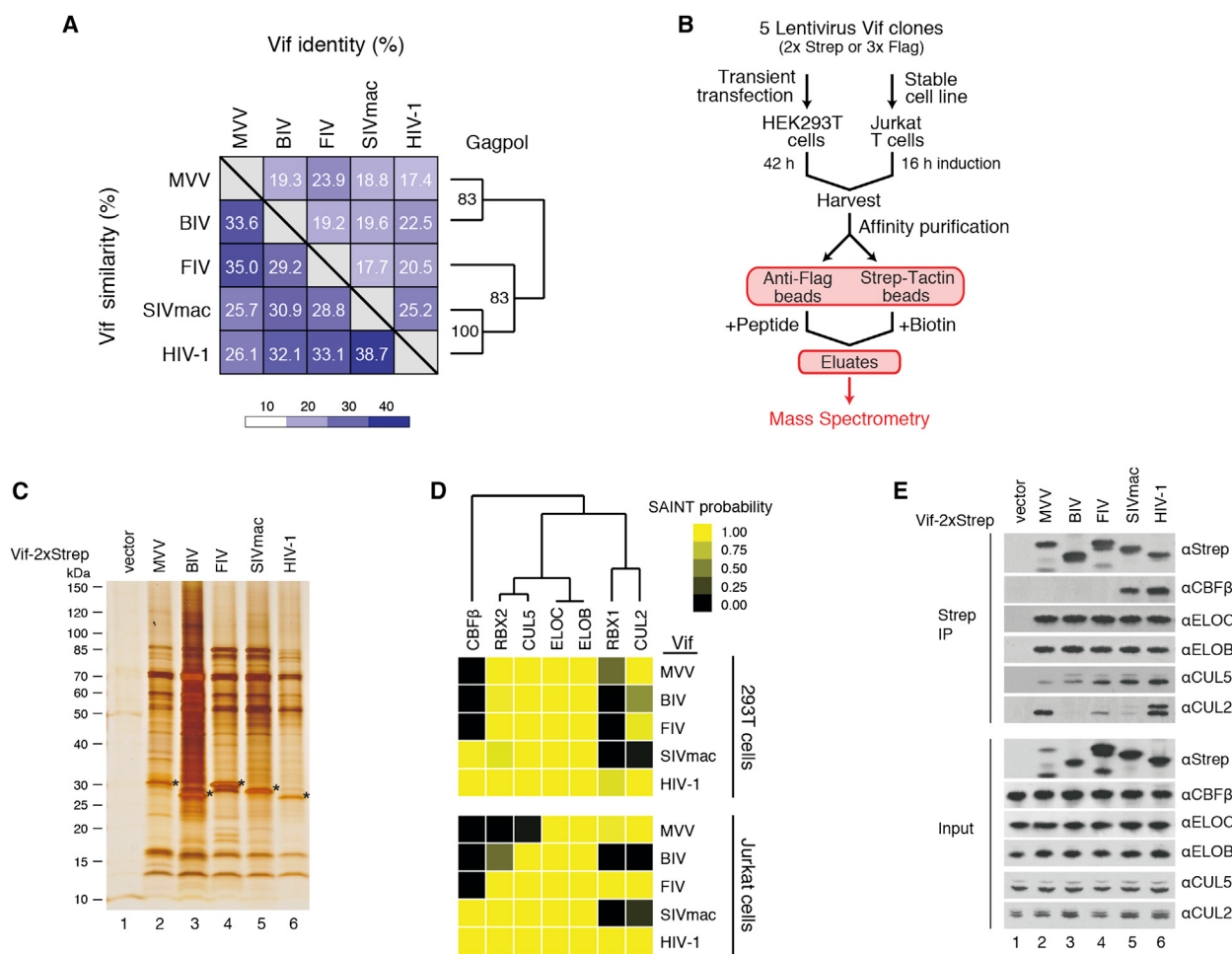


Figure 1. Proteomic Analysis of Lentiviral Vif Proteins

- (A) Percent identity and percent similarity matrix of Vif proteins used in this study. The distance tree was generated from Gagpol protein sequence of viruses, with bootstrap support values.
- (B) Flow chart of affinity purification-mass spectrometry (AP-MS) pipeline used to identify Vif-interacting host proteins.
- (C) Representative silver-stained SDS-PAGE of eluates from a Vif-Strep purification in transiently transfected HEK293T cells. Asterisks indicate Vif proteins.
- (D) Cullin ubiquitin ring ligase (CRL) complex proteins identified in AP-MS experiments, colored by SAINT score and clustered hierarchically by correlation.
- (E) Immunoblot of a Strep affinity purification of Strep-tagged Vif proteins transiently expressed in HEK293T cells, probing for CRL proteins highlighted in (D). See also Figures S1 and S2 and Tables S1 and S2.

(MVV, BIV, and FIV) showed no dependence on CBF β for activity, eliciting equivalent ability to rescue HIV-1 infectivity from A3 restriction both in the presence and in the absence of CBF β (Figures 2D–2F). This finding agrees with recently reported data for MVV, BIV, and FIV Vif proteins (Ai et al., 2014; Han et al., 2014; Zhang et al., 2014a, 2014b).

BIV Vif Assembles a CRL Complex without a Non-canonical Cofactor

Having observed no dependence of the non-primate Vif proteins on CBF β for the *in vivo* degradation of cognate A3 proteins, we asked whether the corresponding Vif-CRL complexes might reconstitute *in vitro* without CBF β or other additional host factors. We have shown previously that HIV-1 Vif requires CBF β to form a stable complex with ELOB and ELOC and CUL5/RBX2 *in vitro* (Figures 2G and 2H; Jäger et al., 2012b). Unexpectedly,

BIV Vif formed a stable trimer with ELOB and ELOC alone with no other cofactors required as assessed by size-exclusion chromatography (Figure 2G). This trimer readily associated with the CUL5/RBX2 scaffold (Figures 2G and 2H) to form an active complex capable of poly-ubiquitylating Myc-tagged bovine A3Z3 (BtA3Z3) (Figure 2I). The level of ubiquitylation was comparable to HIV-1 Vif-CRL-mediated ubiquitylation of Myc-tagged human A3F CTD domain (HsA3F-CTD) (Figure 2I). Reconstitution of active BIV Vif-CRL5 complex thus confirmed that only the endogenous CRL5 complex is required for BIV Vif activity, in stark contrast with the primate lentiviral Vif proteins that require the additional recruitment of CBF β for equivalent activity.

CYPA Implicated as an MVV Vif Host Cofactor

Whereas we successfully reconstituted the BIV Vif-CRL5 complex without a non-canonical host cofactor, we were unable to

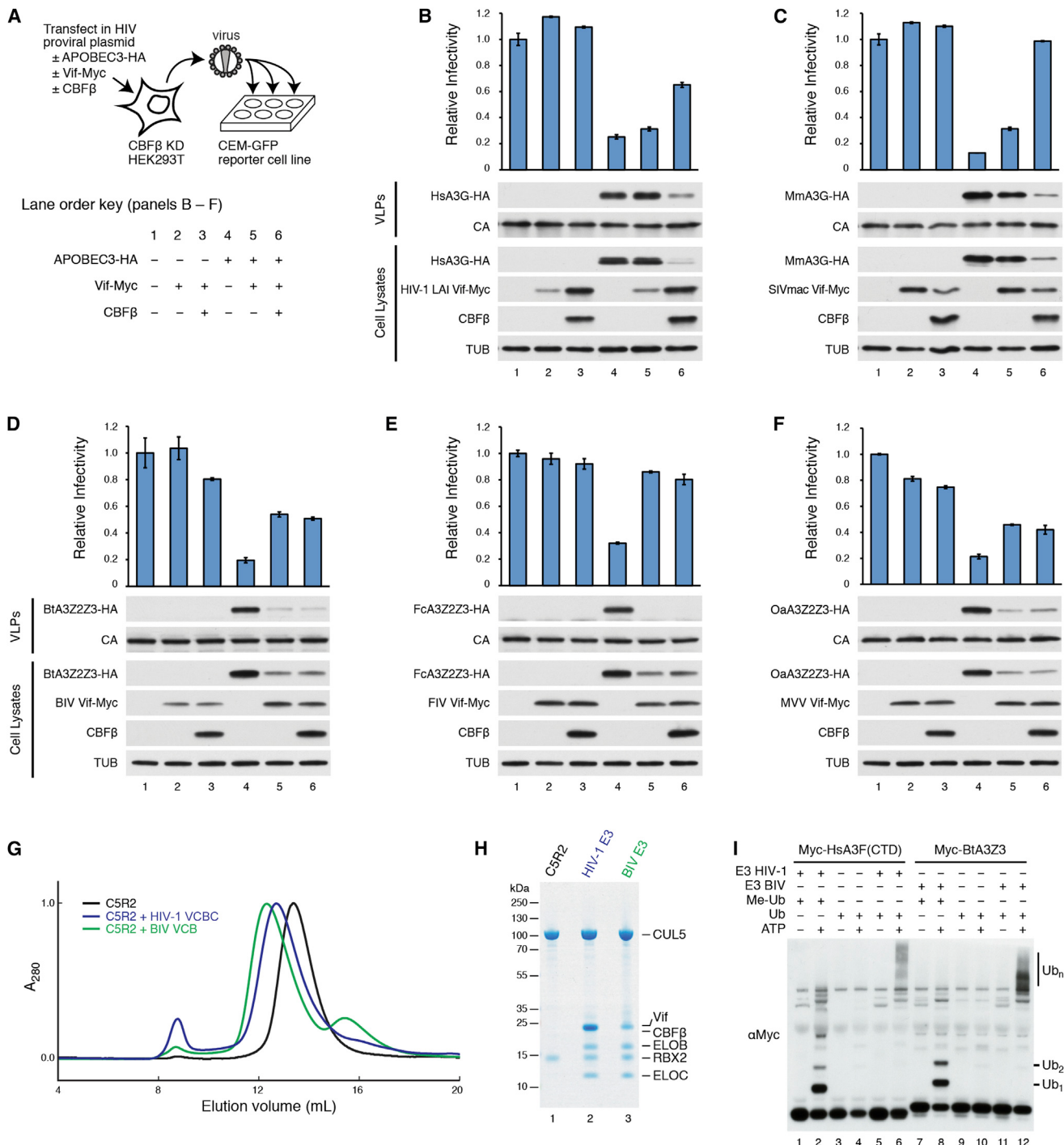


Figure 2. Vif Dependence on CBF β Is Primate Lentivirus Specific

(A) Schema of single-round infection assay.

(B–F) Infectivity assays described in (A), using Vif proteins and cognate A3 proteins. Bars represent mean \pm SE of GFP expression from virus reporter lines. Viral, A3, and CBF β proteins are detected by immunoblot. VLPs, virus-like particles.

(G) UV absorbance curves are shown for gel filtration of CUL5-RBX2 (C5R2) alone or mixed with an excess of indicated Vif complexes (BIV VCB, Vif-ELOB-ELOC; HIV-1 VCBC, Vif-ELOB-ELOC-CBF β). Peaks are observed at earlier elution volumes when C5R2 is mixed with Vif complexes, indicating E3 complex formation.

(H) Coomassie-blue-stained SDS-PAGE of peak fractions collected from gel filtration runs shown in (G).

(I) Immunoblot of ubiquitylation reactions with either HIV-1 Vif or BIV Vif E3, using myc-tagged C-terminal domain of human A3F (Myc-HsA3F CTD) or bovine A3Z3 (Myc-BtA3Z3) as substrate, respectively. Me-Ub, methylated ubiquitin; Ub, ubiquitin.

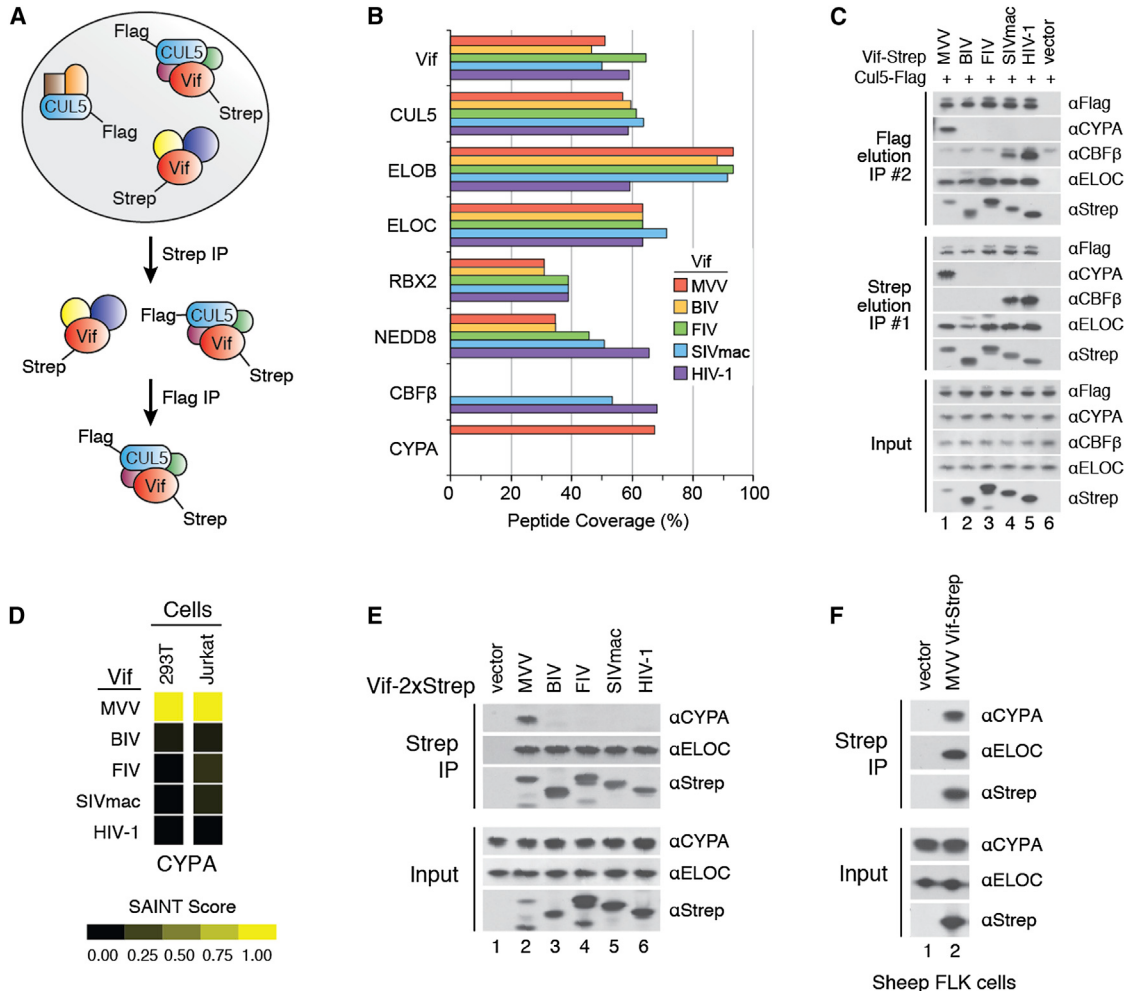


Figure 3. CYPA Is Tightly and Uniquely Associated with MVV Vif

- (A) Cartoon of double affinity purification experiment.
- (B) LC-MS/MS mass spectrometry results from the double purification of 2×Strep-tagged Vif proteins and 3×Flag-tagged CUL5. Bars indicate peptide percent coverage of proteins identified in eluates after second purification step.
- (C) Immunoblot of input lysates and first and second purification eluates used for MS analysis in (B).
- (D) Heatmap of AP-MS data for CYPA in HEK293T and Jurkat T cell lines. Color indicates SAINT score.
- (E) Re-probing of immunoblot of Strep affinity purification shown in Figure 1F; ELOC is shown as a control for CRL complex interaction.
- (F) Strep purification of MVV Vif from transient transfection of ovine FLK cells. CYPA, ELOC, and Vif are detected by immunoblot.

do so with the other non-primate lentiviral Vif complexes (MVV and FIV). Both MVV Vif-ELOB-ELOC and FIV Vif-ELOB-ELOC complexes aggregated during size-exclusion chromatography after purification, mimicking behavior observed with HIV-1 Vif in the absence of CBF β (Figures S3A and S3B; Kim et al., 2013). These data suggested additional host cofactors are required for stable complex formation of the MVV Vif and FIV Vif CRL5 complexes.

To identify the missing components of the non-primate Vif-CRL5 complexes, we utilized a double affinity-tag purification approach (He et al., 2010; Jäger et al., 2012b). We co-transfected HEK293T cells with 2×Strep-tagged Vif proteins and 3×Flag-tagged CUL5 and then performed two-step tandem affinity purification, initially purifying Vif then CUL5 (Figure 3A).

Eluates were then subjected to LC-MS/MS analysis. In each sample, we identified high peptide coverage of the Vif and CUL5 baits as well as of proteins associated with the CRL5 complex (ELOB, ELOC, RBX2, and NEDD8; Figures 3B and 3C). Consistent with our previous data, peptides from CBF β were only observed in the SIVmac and HIV-1 Vif samples. Although we failed to identify likely cofactors in the FIV Vif sample, we did observe a highly abundant non-CRL5 complex host factor in the MVV sample: the peptidyl-prolyl isomerase CYPA (Fischer et al., 1984, 1989; Takahashi et al., 1989; Figures 3B and 3C). CYPA has been reported previously to interact with HIV-1 Capsid (Luban et al., 1993; Thali et al., 1994) but has never before been implicated to play a direct role in Vif biology. Re-examining our Vif single-purification AP-MS data set (Table S2), we

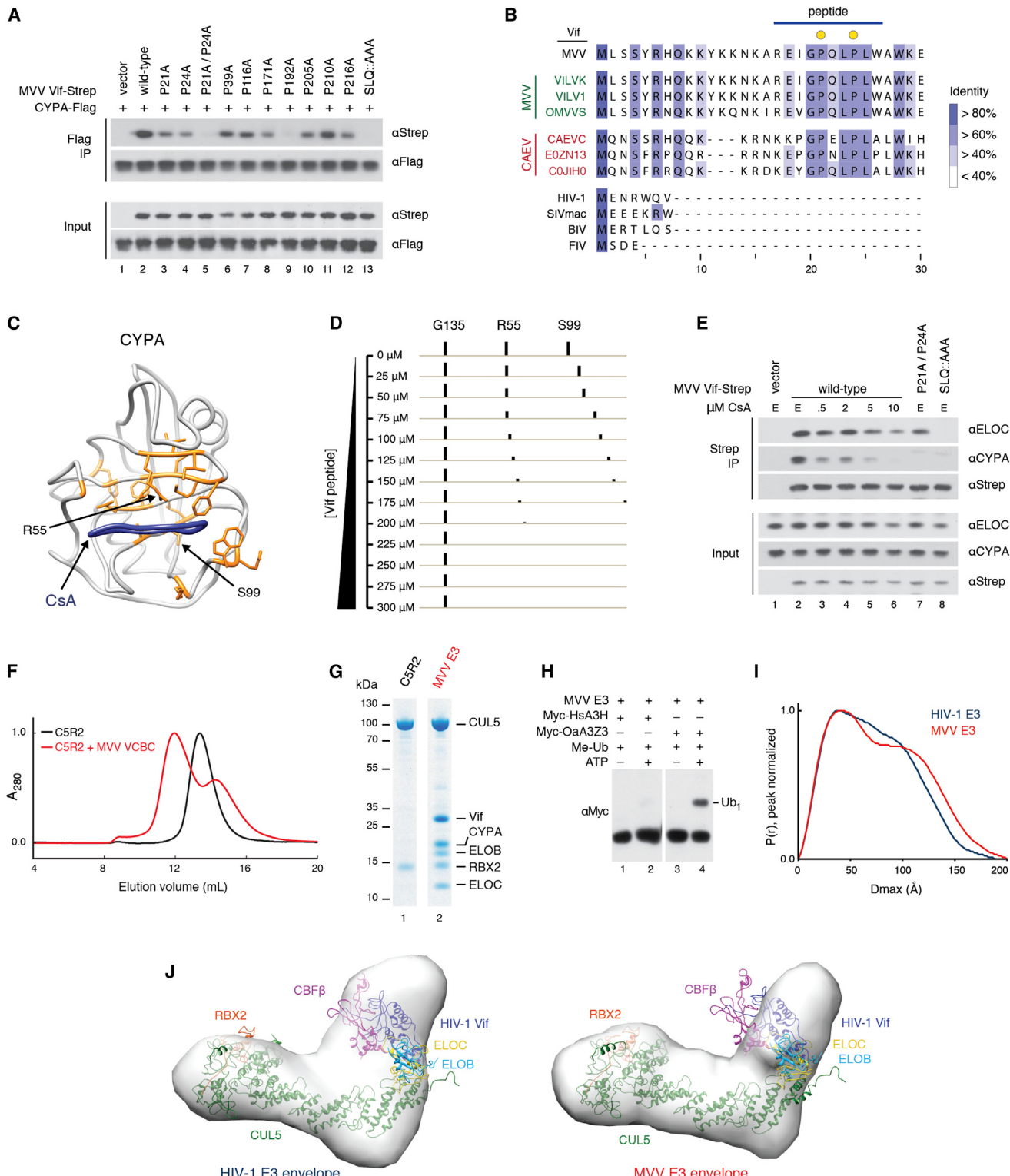


Figure 4. CYPA Is a Component of the MVV Vif-Hijacked CRL Complex

(A) Co-purification testing in vivo interaction between CYPA and either wild-type or mutant MVV Vif. CYPA-Flag and various MVV Vif-Flag constructs are co-transfected, followed by a Flag immunoprecipitation. Co-purification of MVV Vif constructs is assayed by immunoblot.

(B) Multiple sequence alignment of MVV, CAEV, and the other Vif proteins used in this study (BIV, FIV, SIVmac, and HIV-1) referenced to the first 30 amino acids of MVV Vif. Residues P21 and P24 are highlighted, as well as the region used for the CYPA-binding assay in (D). Residues are colored by percent identity.

(legend continued on next page)

observed that CYPA has a specific and highly scoring interaction with only MVV Vif in both HEK293T cells and Jurkat T cells (Figures 3D and 3E). To verify that the CYPA-MVV Vif interaction is not an artifact of expression in human cells, we performed an affinity purification of MVV Vif in natural host sheep (ovine) FLK cells and observed a strong association with endogenous ovine CYPA (Figure 3F).

Identification of MVV Vif Residues P21, P24 as a Likely CYPA Binding Site

After identifying CYPA as a likely member of the MVV Vif-hijacked CRL5 complex, we performed a limited alanine scan of MVV Vif focusing on proline residues, the substrate of CYPA peptidyl-prolyl isomerase activity. We co-expressed Strep-tagged MVV Vif constructs with 3×Flag-tagged CYPA in HEK293T cells and performed a Flag immunoprecipitation, assaying mutants for co-purification of CYPA (Figure 4A). We identified two MVV Vif mutants that were deficient in CYPA binding: P21A/P24A and P192A. In addition, a BC-box mutant (SLQ::AAA) unable to interact with ELOC also was deficient in CYPA binding, suggesting that at least partial assembly of the Vif-hijacked ubiquitin ligase complex is required for stable interaction between MVV Vif and CYPA. We focused on the P21/P24 region as the site of CYPA binding as the sequence is unique within sheep (MVV) and the closely related goat (CAEV)-infecting lentivirus Vif proteins (Figure 4B), whereas the P192 residue is potentially conserved across the broader genus (Figure S1). Indeed, we observe that CAEV Vif is able to co-purify CYPA in an analogous manner to MVV (Figure S4A), confirming our suspicion that the MVV/CAEV clade-specific P21/P24 region is important for CYPA binding.

MVV Vif₂₁PxxP₂₄ Region Binds CYPA Active Site

To determine whether the P21/P24 region of MVV Vif is directly responsible for binding CYPA, we performed NMR shift experiments on CYPA in the presence of a Vif peptide. 2D ¹⁵N-¹H chemical shift correlation spectroscopy was performed on labeled CYPA in the unbound state and in the presence of increasing concentrations of a MVV Vif peptide containing both P21 and P24 (MVV Vif¹⁷⁻²⁶). The addition of the Vif peptide (up to 300 μM) induced significant chemical shift perturbations on the protein spectrum, although saturation was not reached even at the highest Vif concentration and a binding constant could not be determined (Figure 4D). Mapping of the resonances

that disappeared upon addition of the MVV Vif peptide indicated that the peptide binds to the active site of CYPA (Figures 4C and 4D). Additional residues surrounding the active site were observed to enter slow exchange mode or displayed peak broadening (Figure S3C).

To independently verify that MVV Vif interacts with CYPA via the active site of the enzyme, we treated cells expressing 2x Strep-tagged MVV Vif with the CYPA inhibitor cyclosporine A (CsA), which binds to the active site of CYPA and competes for substrate binding (Figure 4C; Takahashi et al., 1989; Thériault et al., 1993). Performing a titration of CsA treatment followed by affinity purification of MVV Vif, we observed a loss of MVV Vif binding to CYPA in the 5–10 μM range, with corresponding weakening of ELOC binding (Figure 4E). The CsA concentration required to disrupt CYPA interaction with MVV Vif is about an order of magnitude greater than our observed concentration required for disrupting the interaction between CYPA and HIV-1 Capsid (Figure S4B). Whereas HIV-1 Capsid binds to CYPA, we find that MVV Capsid does not (Figure S4C). From these experiments, we conclude that MVV Vif binds directly to the CYPA binding site via the ₂₁PxxP₂₄ motif.

CYPA Is Critical for MVV Vif-CRL5 Reconstitution

After observing the CYPA-MVV Vif interaction in vivo, we revisited reconstitution of the MVV Vif-CRL5 complex with the addition of CYPA, in a manner analogous to HIV-1 Vif and CBFβ (Jäger et al., 2012b). CYPA rescued MVV Vif-ELOB-ELOC complex stability (Figures 4F and 4G) and allowed for the formation of a stable complex with CUL5-RBX, capable of ubiquitylating ovine A3Z3, but not human A3H, in vitro (Figure 4H).

To determine whether MVV Vif-CYPA-CRL5 complex conforms to a similar macromolecular organization as the HIV-1 Vif-CBFβ-CRL5 complex, small-angle X-ray scattering (SAXS) analysis was performed on the reconstituted MVV Vif-CYPA-CRL5 complex as well as HIV-1 Vif¹⁻¹⁷⁴-CBFβ-CRL5. Both complexes were monodisperse and well folded under the SAXS experimental conditions, therefore suitable for envelope generation (Figures S5A–S5C). The pairwise distribution function revealed that both HIV-1 and MVV complexes have similar maximal dimensions (Dmax), with values of 190 Å and 200 Å, respectively (Figures 4I; Table S3). Analysis of the resulting envelopes revealed that, despite different complex constituents, the overall surface of the macromolecular assemblies is quite similar with an overall elongated E3 ring-ligase conformation. To

(C) 2D ¹⁵N-¹H chemical shift mapping of CYPA in the presence of MVV Vif¹⁷⁻²⁶ peptide. The resonances of Y48, R55, I56, I57, F60, M61, C62, Q63, G65, G72, L98, S99, A101, Q111, F112, E120, W121, and K125 (orange sticks) shift and then disappear upon addition of the Vif peptide. CsA is labeled in blue. PDB: 1CWA.
(D) Column 1: representative example of a CYPA residue (G135) that is not affected by the presence of the MVV Vif peptide. Column 2: by comparison, R55 and S99 undergo significant chemical shift and intensity reduction. The bars are scaled to the intensity of the HSQC peak at the corresponding Vif concentration.

(E) Affinity purification of MVV Vif in the presence of a titration of CsA. Co-purification of endogenous Vif interactors is assayed by immunoblot. BC-box and proline mutants are used as controls for ELOC and CYPA binding, respectively. E, ethanol.

(F) UV absorbance curves are shown for gel filtration of CUL5-RBX2 (C5R2) alone or mixed with an excess of indicated Vif complexes (MVV VCBC, Vif-ELOB-ELOC-CYPA). Peaks are observed at earlier elution volumes when C5R2 is mixed with Vif complexes, indicating E3 complex formation.

(G) Coomassie-blue-stained SDS-PAGE of peak fractions collected from gel filtration runs shown in (F).

(H) Immunoblot of methyl-ubiquitylation reactions with MVV E3 and either myc-tagged human A3H (Myc-HsA3H) or ovine A3Z3 (Myc-OaA3-Z3).

(I) Pair distance distribution function, P(r), calculated from SAXS intensity data.

(J) Molecular envelopes of HIV-1 Vif¹⁻¹⁷⁴-CBFβ-CRL5 (left) and MVV Vif-CYPA-CRL5 (right) calculated from P(r). An HIV-1 E3 model was superimposed into both envelopes.

See also Figures S3 and S5 and Table S3.

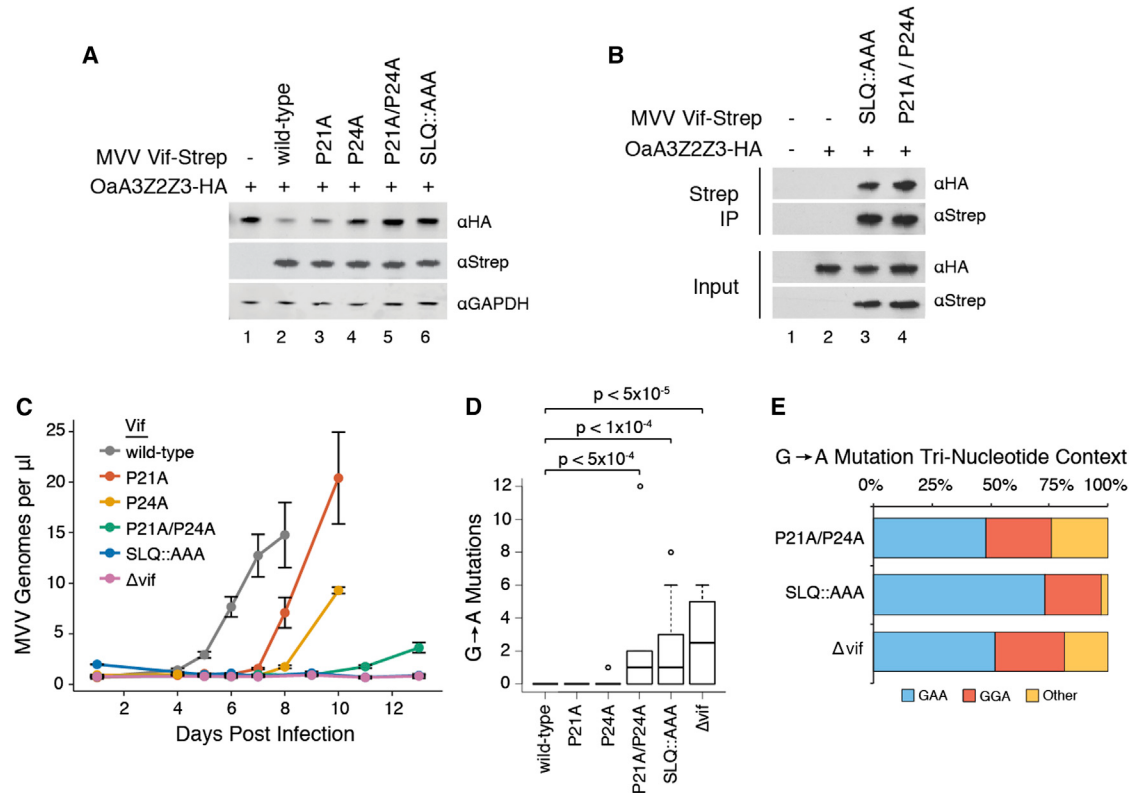


Figure 5. MVV Vif Mutants Deficient in CYPA Binding Are Deficient in A3 Antagonism and Cannot Promote MVV Infectivity In Situ

(A) Co-transfection of HA-tagged ovine A3Z2Z3 (OaA3Z2Z3-HA) and either wild-type or proline mutant MVV Vif. A3 stability in the presence of Vif is assayed by immunoblot.

(B) Co-affinity purification between OaA3Z2Z3 and MVV Vif constructs that were deficient in OaA3Z2Z3 destabilization in (A). Interaction between A3 and Vif proteins is assayed by immunoblotting.

(C) MVV spreading assay in ovine primary macrophage cells. Lysates were harvested at various time points post-infection, and virus genome copies were quantified using TaqMan-based real-time PCR, mean \pm SE ($n = 3$).

(D) Hypermutation assay of MVV strain KV1772. MVVs with either wild-type or mutant *vif* were subjected to a single-cycle infection assay in primary sheep choroid plexus (SCP) cells, and produced viruses were then used to infect SCP cells, generated pro-viruses cloned, and assayed for A3-mediated G-to-A mutations. Wild-type, P24A: $n = 20$; P21A: $n = 16$; P21A/P24A: $n = 17$; SLQ::AAA: $n = 19$; Δvif: $n = 10$. Significance values were determined by a one-sided Wilcoxon rank-sum test compared to wild-type; no annotated p value indicates p value > 0.05 .

(E) Tri-nucleotide context of G-to-A mutations measured in (C). Other refers to any GNN tri-nucleotide other than GGA or GAA.

See also Figure S6.

determine how well the SAXS envelopes fit the available structure data, a model of HIV-1 Vif-CRL5 was generated. Whereas the HIV-1 Vif-CRL5 model was relatively well fit into its experimental SAXS envelope, with a chi value of 1.89 (Figure S5D), there was a slightly poorer fit into the experimentally determined MVV Vif-CRL5 envelope, possibly due to differences in substrate receptor structure (Figure 4J). This likely reflects different folding of CYPA and CBF β and possibly of MVV and HIV-1 Vif proteins.

Correlated Deficiencies in CYPA Binding and A3 Antagonism in MVV Vif Mutants

We next asked whether CYPA also affected MVV Vif A3 degradation activity. Focusing our analysis on the P21, P24 putative CYPA binding site, we co-expressed 3xHA-tagged ovine A3Z2Z3 (OaA3Z2Z3) with 2xStrep-tagged wild-type, P21A, P24A, P21A/P24A, and SLQ::AAA MVV Vif mutants and observed that the loss of CYPA binding to these mutants corre-

lated with reduction in OaA3Z2Z3 degradation activity (Figure 5A). To determine whether the loss-of-function MVV Vif mutants were deficient in forming active CRL complexes or merely unable to bind substrate due to structurally compromising mutations, we performed co-affinity purification experiments with Strep-tagged MVV Vif mutants in the presence of HA-tagged OaA3Z2Z3. We observed that both mutants deficient in A3 degradation activity (P21A/P24A and SLQ::AAA) bound OaA3Z2Z3 (Figure 5B), indicating that the mutations prevent proper assembly of a functional CRL complex without disrupting substrate binding.

To test the importance of the MVV Vif-CYPA interaction for viral infectivity in vivo, we performed a spreading infection with MVV strain KV1772 in primary sheep macrophages with wild-type, P21A, P24A, P21A / P24A, or *vif*-null strains. Whereas all mutants showed reproducibly diminished spreading kinetics compared to wild-type virus, the P21A/P24A mutant showed a

greater spreading defect than the individual P21A and P24A mutations, copying the severe spreading defect observed with the SLQ::AAA and *vif*-null viruses (Figure 5C). The assay was also performed in primary sheep choroid plexus (SCP) cells with similar results (Figure S6E). After spread, we cloned and sequenced the integrated proviruses in each infection to determine whether viral restriction correlated with G-to-A mutational load indicative of A3 antiviral activity. We observed significant increases in G-to-A mutations in P21A/P24A ($p = 1.41 \times 10^{-4}$), SLQ::AAA ($p = 5.27 \times 10^{-5}$), and Δvif ($p = 1.84 \times 10^{-5}$) MVV compared to wild-type using a one-sided Wilcoxon rank-sum test (SCP cell results; Figure 5D). No significant increase in mutations was observed for either the P21A or the P24A single mutations relative to wild-type (Figures 5D and S7A–S7C). The tri-nucleotide sequence preferences of the G-to-A mutations were similar across all conditions (G(G/A)A), again strongly indicative of A3-mediated mutation (Figures 5E and S7D).

CYPA Is Required for Ovine A3 Degradation by MVV Vif

We tested MVV Vif dependence on CYPA for A3 degradation activity using a CYPA knockdown in human cells but were unable to achieve a knockdown sufficient to prevent either OaA3 degradation or MVV Vif-CRL complex formation using polyclonal lines (data not shown). Titration experiments using CsA showed limited but reproducible inhibition of OaA3Z2Z3 degradation by MVV Vif, increasing with CsA concentration until about 5 μM when toxicity became apparent (Figure S4B). Importantly, the inhibition was not observed with HIV-1 Vif and its cognate substrate, human A3G (HsA3G) (Figure S4C).

Due to lack of efficacy of either CYPA knockdowns or CsA treatments individually, we attempted to inhibit MVV Vif by combining both protocols, treating a monoclonal CYPA knockdown line with 2 μM CsA and comparing MVV Vif A3 degradation activity to a non-targeting control line. We observed a modest inhibition of Vif-mediated OaA3Z2Z3 degradation in the knockdown line compared to the control line without CsA treatment. In contrast, we observe near-complete inhibition of MVV Vif degradation activity in CYPA knockdown cells treated with CsA (Figure 6A, lanes 9 and 10). HIV-1 Vif A3 degradation activity was not affected by CsA treatment in either the knockdown or the control line (Figure S4D), indicating the combination of CYPA knockdown and CsA treatment was specifically and cooperatively interfering with the MVV Vif-CYPA interaction.

Given that drug and shRNA treatments can have off-target effects, we next performed ovine A3 degradation assays in an isogenic system using a Jurkat T cell line and CYPA^{−/−} knockout (KO) line (Braaten and Luban, 2001). Immunoblots confirmed the lack of CYPA expression in the Jurkat CYPA^{−/−} KO line compared to the parental Jurkat E6-1 CYPA^{+/+} line (Figure 6B). The KO line or the parental line was then nucleofected with an HA-tagged OaA3Z2Z3 expression construct in the presence or absence of Strep-tagged MVV Vif and Flag-tagged CYPA complementation (Figure 6B). We observe a complete loss of MVV Vif-mediated degradation of OaA3Z2Z3 in the CYPA^{−/−} KO line (Figure 6C, top, lanes 5 and 6), which can be rescued upon complementation with exogenous CYPA (Figure 6C, top, lanes 7 and 8). We were unable to detect expression of MVV Vif in the CYPA^{−/−} KO line without exogenous CYPA comple-

mentation, suggesting MVV Vif stability depends on CYPA presence in vivo. This closely mimics the stability requirements of HIV-1 Vif on CBFβ and is consistent with our in vitro reconstitution results with MVV Vif. We did not observe any dependence on exogenous CYPA expression for MVV Vif A3 degradation activity in the parental Jurkat E6-1 CYPA^{+/+} line (Figure 6C, bottom) and did not observe any dependence on CYPA for A3 degradation activity for HIV-1 Vif and HsA3G in either cell line (Figure 6D).

Lastly, we assessed whether or not various active-site mutants of CYPA could also rescue MVV function in the KO background. We tested three CYPA mutants—R55K, F113W, and H126A—all located within the active site of CYPA and previously reported to affect activity (Figure S7A; Bosco et al., 2010). We found that two mutants, R55K and F113W, failed to rescue MVV Vif A3 degradation activity in the CYPA^{−/−} KO line and that a third mutant, H126A, was able to rescue activity as efficiently as wild-type CYPA (Figure 6E). Similar results were obtained in the monoclonal CYPA knockdown line (Figure S7B). We additionally tested the CYPA mutants for MVV Vif binding through in vitro reconstitution and found that all three were capable of forming a stable MVV Vif-ELOB-ELOC-CYPA complex (Figures S7C and S7D). Whereas it is possible that the lack of R55K and F113W rescue of MVV Vif activity is due to a weakening of binding in vivo, the in vitro binding data suggest CYPA isomerase activity is important for MVV Vif A3 degradation activity.

DISCUSSION

The retrovirus family infects a diverse set of mammalian hosts, with each viral lineage required to evolve a mechanism to overcome the host challenge to infection presented by A3 proteins. Solutions to this A3 host challenge by retroviruses include the lentivirus protein Vif that induces the proteasomal degradation of A3 proteins (Larue et al., 2010; Sheehy et al., 2002; Yu et al., 2003), sequestration of A3 proteins away from virions by the foamy virus protein Bet (Löchelt et al., 2005), or preventing A3 binding to virion proteins in HTLV-1 (Derse et al., 2007). Even within lentiviruses, the equine infectious anemia virus has evolved a Vif-independent, non-degrading mechanism of escaping A3 restriction (Bogerd et al., 2008). Through a series of proteomic, virological, biochemical, and structural approaches targeting five evolutionarily distinct lentiviral Vif proteins from HIV-1, SIVmac, MVV, BIV, and FIV, we present data consistent with a model of high biochemical plasticity at the molecular level but “modular conservation” due to their conserved function of ubiquitylation and subsequent proteasomal degradation of host A3 restriction factors (Figure 7).

Using AP-MS, we identified a conserved core ubiquitin ligase complex—CUL5-ELOB-ELOC-RBX2—involved in Vif-mediated degradation of host A3 proteins. For a functional complex, HIV-1 and SIVmac Vif proteins additionally require the host cofactor CBFβ for both complex assembly and activity (Han et al., 2014; Hultquist et al., 2012; Zhang et al., 2012). Our data both identify the CBFβ interaction with HIV-1 and SIVmac Vif proteins and demonstrate their dependence on this cofactor for A3 degradation activity. The interaction with CBFβ was not observed by AP-MS nor was it functionally required for A3

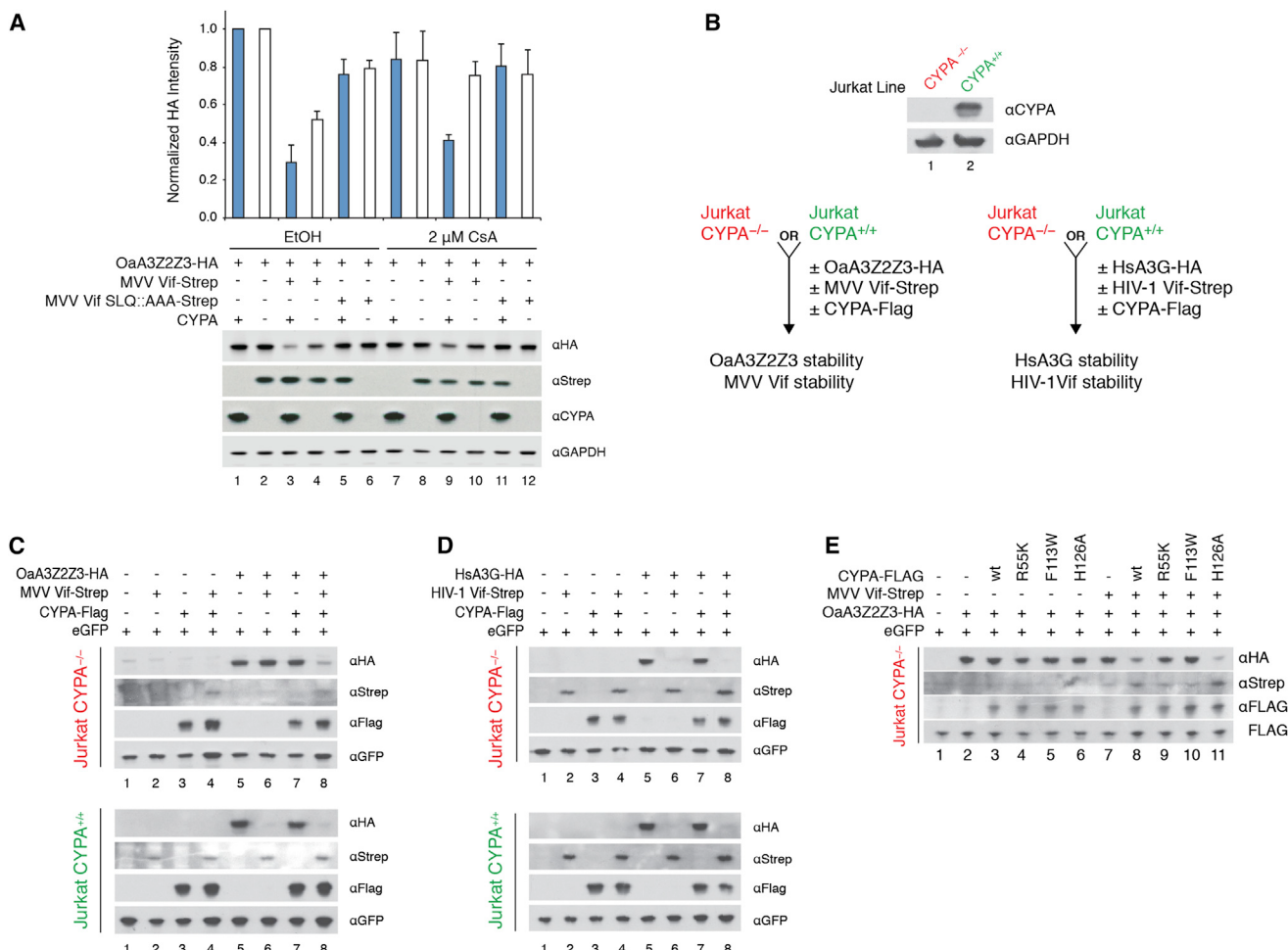


Figure 6. CYPA Is Required for MVV Vif A3 Degradation Activity

(A) Comparison of Vif A3 degradation activity in monoclonal CYPA knockdown versus control cells in the presence or absence of CsA. Cells were transiently transfected with HA-tagged ovine A3Z2Z3 (OaA3-Z2Z3) and either wild-type or BC-box mutant (SLQ::AAA) Strep-tagged MVV Vif and then treated 6 hr later with either ethanol (E) or 2 μ M CsA overnight. Bars represent HA immunoreactivity normalized first by GAPDH loading control and then to no Vif control for each cell line; mean \pm SE ($n = 3$). Proteins are detected by immunoblotting.

(B) CYPA immunoblot in Jurkat E6-1 CYPA^{+/+} "parental" line and derived E6-1 CYPA^{-/-} knockout (KO) line.

(C) Top: Jurkat CYPA^{-/-} KO cells are transiently transfected with HA-tagged OaA3Z2Z3, Strep-tagged MVV Vif, and Flag-tagged CYPA. eGFP is used as transfection control. Bottom: identical experiment performed in E6-1 CYPA^{+/+} control line.

(D) Top: Jurkat CYPA^{-/-} KO cells are transiently transfected with HA-tagged human A3G (HsA3G), Strep-tagged HIV-1 Vif, and Flag-tagged CYPA. eGFP is used as transfection control. Bottom: identical experiment performed in E6-1 CYPA^{+/+} control line.

(E) MVV Vif activity rescue assay using mutants of CYPA. Strep-tagged MVV Vif, HA-tagged OaA3Z2Z3, and various Flag-tagged CYPA constructs are transfected into Jurkat CYPA^{-/-} KO line and Vif activity assessed through A3 stability.

See also Figures S4 and S7.

degradation activity in the non-primate lentiviral Vif proteins, consistent with recent observations (Ai et al., 2014; Han et al., 2014; Zhang et al., 2014a, 2014b). We identified one non-primate lentivirus, BIV, with a Vif protein that requires no non-canonical host cofactor for both complex assembly and activity in vitro and identified another, MVV, with a Vif protein that requires a novel non-canonical host cofactor, CYPA, to play a CBF β -like role in regulating ligase assembly and activity both in vitro and in vivo. Though no FIV Vif cofactor was identified, we cannot exclude the possibility that it requires an as of yet unidentified one.

Interaction of MVV Vif with the Non-canonical Cofactor CYPA

The interaction between MVV Vif and CYPA appears to be unique among the lentiviruses examined in this study. Through a combination of targeted mutagenesis and NMR spectroscopy, we identified a di-proline motif in the N terminus of MVV Vif, $_{20}$ GPQLP $_{24}$, which directly binds the CYPA active site. This site is uniquely found in MVV and the closely related CAEV Vif proteins (Figure 4B). The motif bears some resemblance to the CYPA binding site of HIV-1 Capsid, $_{89}$ GPIAP $_{93}$ (Gamble et al., 1996), a GPxxP motif. However, the strength of the interaction

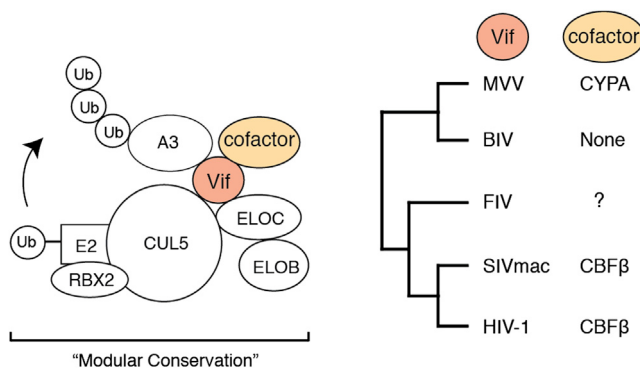


Figure 7. Modular Conservation of CRL Hijacking and Non-canonical Cofactor Recruitment by Vif

The host CRL complex hijacked by Vif represents a conserved host-pathogen interaction module. Vif proteins recruit non-canonical host cofactors in a lineage-specific manner within the lentivirus genus. Tree from Figure 1A.

between MVV Vif and CYPA appears to be much greater than that of CYPA and HIV-1 Capsid as assessed by interaction disruption by CsA treatment (Figures 4E and S5A). Further to this point, the relatively low affinity measured by NMR spectroscopy between CYPA and MVV Vif^{17–28} peptide is incompatible with the observed stability of the reconstituted MVV Vif-ELOB-ELOC-CYPA complex. These data suggest the existence of binding surfaces on MVV Vif in addition to the identified di-proline motif and these surfaces are likely outside of the active site of CYPA as evidenced by the inefficacy of CsA treatment in disrupting MVV Vif-CYPA interaction or inhibiting MVV Vif anti-A3 activity without complementary knockdown of CYPA (Figure 6A).

Cellular chaperones interact with a large contingent of clients to catalyze their folding and often interact with their substrates via general features, such as hydrophobic patches, rather than specific PPI surfaces or domains (Jaya et al., 2009; Spiess et al., 2006). The relatively promiscuous interactions of CYPA combined with a high cellular concentration may have eased the evolution of MVV Vif to capture CYPA. If the interaction between the two proteins is mechanistically unrelated to perturbing endogenous CYPA activities, this may explain the selection of CYPA by the virus. The capture of CYPA by MVV Vif would involve transition of the CYPA interaction from a potentially catalytic one in aiding Vif folding to a stoichiometric one in forming a stable complex. The importance of CYPA catalytic function for MVV Vif appears to be retained, as two CYPA active-site mutants appear to bind MVV Vif without forming an active A3-degrading complex (Figure 6E). The one CYPA mutant that was not deficient in this activity, H126A, had been previously shown to be active with an HIV-1 Capsid substrate (Bosco et al., 2010). This model of capture would likely not apply to the interaction between primate lentiviral Vif proteins and CBFβ, as the interaction falls in a specific PPI surface evolved by CBFβ to interact with the runt domain of RUNX transcription factors (Guo et al., 2014).

Cofactor Acquisition as Gain-of-Function Adaptations

Whereas we cannot definitively infer the ancestral form of Vif-hijacked CRL complex, parsimony suggests the ancestral form would resemble the BIV Vif-hijacked complex. BIV Vif most re-

sembles an endogenous BC-box E3 substrate adaptor, which binds CRL2/5 complexes without the need of non-canonical cofactors. The parsimony model would imply that the interactions between Vif and non-canonical host cofactors (MVV-CYPA; HIV-1/SIVmac-CBFβ) are derived interactions that occurred independently during the evolution of modern lentiviruses. Why these interactions evolved or what selective advantage they may grant to the viruses remains unclear. We previously suggested that the interaction between HIV-1 Vif and CBFβ may disrupt the endogenous activities of RUNX transcription factors (Jäger et al., 2012b) and have shown Vif-mediated interference of RUNX-controlled genes in T-lymphocytes (Kim et al., 2013). This “dual-hijacking” may also exist for the MVV-CYPA interaction, although it is worth noting that CYPA is a highly abundant protein in virtually every cell type, and therefore the secondary effect would necessarily be one that required relatively small changes in cellular CYPA abundance or involve local effects proximate to MVV Vif activity.

Another driving force in the evolution of novel Vif cofactors is the evolution of the viral proteins’ substrates, the A3 family. The number of A3 genes in a given mammalian genome varies widely, from only a single gene in mice to seven members in primates (Bogerd et al., 2008; Jarmuz et al., 2002; LaRue et al., 2008; Münk et al., 2008). The acquisition of CBFβ as a Vif cofactor by primate lentiviruses coincides with the expansion of A3 family of proteins in primates, and it is possible that the cofactor acquisition enabled Vif to preserve viral fitness without the need to evolve another, non-CRL mechanism to recognize and degrade the larger A3 substrate repertoire (Ai et al., 2014). A recent structure of the SIV/HIV-2 accessory factor Vpx showed the co-crystallized Cullin-4A adaptor protein DCAF1 directly contacts the viral substrate SAMHD1 (Schwefel et al., 2014); this example may be generalizable to a model of host factors extending the viral E3 surface for substrate recognition. The A3 expansion-driving cofactor acquisition model would fail to explain the interaction between MVV Vif and CYPA, as the ovine genome shows no increase in the number of A3 proteins compared with the bovine genome and one less than the feline genome (LaRue et al., 2008; Münk et al., 2008). Interestingly, MVV Vif is observed to have a high promiscuity for A3 proteins, showing activity against many non-cognate A3s (Larue et al., 2010), potentially supporting a model of cofactor-mediated substrate expansion.

An intriguing possibility is that non-canonical cofactors act to increase the evolvability of their Vif partner, enabling Vif proteins to retain activity with otherwise lethal mutations during transitions to more-fit states. Restriction factors are a major barrier to zoonosis (Sharp and Hahn, 2011), and a Vif protein able to adapt more quickly to a new host’s A3 proteins should grant the lentivirus a competitive advantage in zoonotic transmission, as well as in populations with diverse restriction factor haplotypes (Binka et al., 2012; Ooms et al., 2013). Whether gaining an interaction partner makes a viral protein more robust to mutation is debatable, as the benefits of stabilization via the interaction may be outweighed by the mutational constraints imposed by the interaction itself. HIV-1 Vif must maintain direct interactions with ELOC, CUL5, multiple A3 proteins, and a large surface with CBFβ to be functional, yet even after the establishment of

the interaction between CBF β and primate lentivirus Vif, it has recently undergone dramatic sequence changes (Etienne et al., 2013).

CYPA Potentially Bridges Vif Antagonism of A3 with TRIM5 Escape

We explored the idea of whether or not the interaction between CYPA and MVV Vif may be related to the genetic conflict between lentiviruses and the host restriction factor TRIM5 (Strem-lau et al., 2004). In HIV-1, CYPA interaction with the viral capsid is involved in mitigating the antiviral actions of TRIM5 (Sokolskaja and Luban, 2006), and some old world primate hosts have evolved a TRIM5-CYPA fusion protein, TRIMCyp, which uses its CYPA domain to recruit the TRIM5 domain to the viral core (Nisole et al., 2004; Sayah et al., 2004). MVV is restricted by sheep TRIM5 when overexpressed in cell culture, but the mechanism by which MVV avoids this restriction in vivo is unknown (Jáuregui et al., 2012). It remains possible that the interaction between CYPA and MVV Vif is to allow crosstalk of Vif between two different host restriction pathways—A3 and TRIM5—particularly if there exists an as of yet unidentified TRIMCyp gene in the sheep genome.

In addition to its role in TRIM5-mediated restriction, the interaction of CYPA with HIV-1 Capsid has recently been found to be essential for the virus to evade detection by the innate immune sensor cGAS and to avoid subsequent activation of the innate immune response (Lahaye et al., 2013; Rasaiyah et al., 2013). Intriguingly, a pair of mutants in MVV Vif and Capsid (P205S and L120R, respectively) results in a restricted growth phenotype, whereas neither mutant alone impacts replication (Gudmundsson et al., 2005). Whether or not this is related to the MVV Vif interaction with CYPA is under investigation.

Modular Conservation and Lineage-Specific Interactions

We have shown that, despite a generally conserved mechanism of mediating host A3 degradation by ubiquitylation and subsequent proteasomal degradation, lentiviruses demonstrate surprising plasticity in the biochemical requirements for this activity through their Vif proteins. Whereas other lentiviruses have been observed to change viral protein-host substrate interactions (Lim et al., 2012; Sauter et al., 2009) or the sites of substrate recognition (Fregoso et al., 2013), Vif is unique in that the viral protein substrate and the core machinery required for activity appear to be conserved and yet cofactor interaction partners are varied and lineage specific. We have previously noted this concept of modular conservation where the function of biochemical modules is conserved but the underlying molecular interactions between the modules have changed significantly. For example, we have shown that, although genetic interactions between different species have evolved rapidly, the genetic relationships within protein complexes, or modules, are highly conserved (Beltrao et al., 2010; Roguev et al., 2008; Ryan et al., 2012). In this vein, it remains to be seen whether or not the Vif paradigm is generalizable, but it is clear that viral proteins, even in the context of “stable” interactions with host factors, can still undergo rapid and surprisingly dramatic changes over the course of virus evolution.

EXPERIMENTAL PROCEDURES

Detailed experimental procedures are available in the [Supplemental Experimental Procedures](#).

Expression Constructs

HIV-1_{LAI}, SIV_{mac239}, BIV, FIV, and MVV *vif* constructs in pVR1012 (Vical) have been reported previously (Larue et al., 2010).

Ovine Cells and MVV Infections

SCP cells and sheep-blood-derived macrophages were infected with RT-normalized wild-type and mutant viruses for spreading infection assays. Samples were taken daily for Taqman qPCR.

Affinity Purifications

Affinity purifications (AP) were generally performed as described previously (Jäger et al., 2012a).

Mass Spectrometry Data and Analysis

Digested peptide mixtures were analyzed on either a Thermo Scientific Velos Pro or a Thermo Scientific LTQ XL ion trap mass spectrometry system. Data were searched against a database containing SwissProt human protein sequences. Interactions were scored using the SAINT algorithm (Choi et al., 2011) with prey-identified spectral counts.

In Vitro Reconstitution and Ubiquitylation Assays

Vif complexes for in vitro work were produced by co-expression in BL21-Star(DE3)pLysS cells. CUL5-RBX2 and all ubiquitin and Nedd8 pathway components used in ubiquitylation assays were obtained as previously described (Stanley et al., 2012).

CYPA Knockdown and Cyclosporine Treatment

CYPA knockdown lines were generated in HEK293T cells using pLKO.1-derived lentiviruses encoding an shRNA-targeting CYPA (TRCN0000049277). For assays involving CsA (no. 9973; Cell Signaling Technology), cells were treated with 2–5 μ M CsA 4–6 hr post-transfection to prevent potential loss in transfection efficiency.

SUPPLEMENTAL INFORMATION

Supplemental Information includes Supplemental Experimental Procedures, seven figures, and three tables and can be found with this article online at <http://dx.doi.org/10.1016/j.celrep.2015.04.038>.

AUTHOR CONTRIBUTIONS

J.R.K. conceived the project with N.J.K. and R.S.H., performed affinity purifications, scored mass spectrometry data, created stable cell lines, and performed CsA assays, knockdown assays, and Jurkat nucleofection experiments. D.J.S. performed in vitro reconstitution of Vif-CRL complexes and ubiquitylation assays. J.F.H. performed single-cycle HIV-1 infectivity assays and assisted with Jurkat nucleofection experiments. J.R.J., B.W.N., T.L.J., and K.E.F.-S. performed MS sample preparation, machine runs, and data searching. N.M., S.R.J., H.I.G., and A.A. performed MVV virology assays. J.M.B. generated SAXS envelopes of Vif-CRL5 complexes. S.B. performed NMR experiments. M.L. purified A3 proteins for in vitro ubiquitylation assays. W.L.B. sequenced MVV proviral sequences for hypermutation assays. J.R.K. wrote the manuscript with assistance from J.F.H. and N.J.K. Manuscript editors were J.R.K., D.J.S., J.F.H., J.M.B., S.B., J.S.F., R.S.H., V.A., J.D.G., and N.J.K.

ACKNOWLEDGMENTS

The authors wish to thank members of the N.J.K., J.D.G., J.S.F., R.S.H., and V.A. labs; P. Hartley for assisting in stable line generation; R. LaRue for cloning of MVV, BIV, FIV, and SIVmac Vif plasmids; S. Jäger, S. Chen, M. Eckhardt, and D. Gordon for reagents; Z. Rizvi for CYPA cloning; S.J., C. Mahon, and

G. Jang for expertise and advice in affinity purifications; E. Verschueren and P. Cimermančič for advice on AP-MS scoring; and M. Shales for assistance in figure construction. We would kindly thank S.J. Kim for help in collecting SAXS profiles and D. Schneidman for her assistance in generating the HIV E3 model and analyzing the SAXS data using the AllosMod-FoXS server. The following reagents were obtained through the NIH AIDS Reagent Program, Division of AIDS, NIAID, NIH: Jurkat Clone E6-1 from Dr. A. Weiss and Jurkat T cells CYPA^{-/-} from Drs. D. Braaten and J. Luban. J.R.K. was supported by an NSF graduate research fellowship. This work was supported by NIH grants to N.J.K (P50 GM082250, P50 GM081879, and P01 AI090935) and to R.S.H. (R01 AI064046 and P01 GM091743) and a grant from the Icelandic Research Fund to V.A. (141085-051).

Received: October 21, 2014

Revised: March 13, 2015

Accepted: April 18, 2015

Published: May 14, 2015

REFERENCES

- Al, Y., Zhu, D., Wang, C., Su, C., Ma, J., Ma, J., and Wang, X. (2014). Core-binding factor subunit beta is not required for non-primate lentiviral Vif-mediated APOBEC3 degradation. *J. Virol.* 88, 12112–12122.
- Beltrao, P., Cagney, G., and Krogan, N.J. (2010). Quantitative genetic interactions reveal biological modularity. *Cell* 141, 739–745.
- Binka, M., Ooms, M., Steward, M., and Simon, V. (2012). The activity spectrum of Vif from multiple HIV-1 subtypes against APOBEC3G, APOBEC3F, and APOBEC3H. *J. Virol.* 86, 49–59.
- Bogerd, H.P., Tallmadge, R.L., Oaks, J.L., Carpenter, S., and Cullen, B.R. (2008). Equine infectious anemia virus resists the antiretroviral activity of equine APOBEC3 proteins through a packaging-independent mechanism. *J. Virol.* 82, 11889–11901.
- Bosco, D.A., Eisenmesser, E.Z., Clarkson, M.W., Wolf-Watz, M., Labeikovsky, W., Millet, O., and Kern, D. (2010). Dissecting the microscopic steps of the cyclophilin A enzymatic cycle on the biological HIV-1 capsid substrate by NMR. *J. Mol. Biol.* 403, 723–738.
- Braaten, D., and Luban, J. (2001). Cyclophilin A regulates HIV-1 infectivity, as demonstrated by gene targeting in human T cells. *EMBO J.* 20, 1300–1309.
- Choi, H., Larsen, B., Lin, Z.-Y., Breitkreutz, A., Mellacheruvu, D., Fermin, D., Qin, Z.S., Tyers, M., Gingras, A.-C., and Nesvizhskii, A.I. (2011). SAINT: probabilistic scoring of affinity purification-mass spectrometry data. *Nat. Methods* 8, 70–73.
- Davis, Z.H., Verschueren, E., Jang, G.M., Kleffman, K., Johnson, J.R., Park, J., Von Dollen, J., Maher, M.C., Johnson, T., Newton, W., et al. (2015). Global mapping of herpesvirus-host protein complexes reveals a transcription strategy for late genes. *Mol. Cell* 57, 349–360.
- Derse, D., Hill, S.A., Princler, G., Lloyd, P., and Heidecker, G. (2007). Resistance of human T cell leukemia virus type 1 to APOBEC3G restriction is mediated by elements in nucleocapsid. *Proc. Natl. Acad. Sci. USA* 104, 2915–2920.
- Etienne, L., Hahn, B.H., Sharp, P.M., Matsen, F.A., and Emerman, M. (2013). Gene loss and adaptation to hominids underlie the ancient origin of HIV-1. *Cell Host Microbe* 14, 85–92.
- Fischer, G., Bang, H., and Mech, C. (1984). [Determination of enzymatic catalysis for the cis-trans-isomerization of peptide binding in proline-containing peptides]. *Biomed. Biochim. Acta* 43, 1101–1111.
- Fischer, G., Wittmann-Liebold, B., Lang, K., Kiehaber, T., and Schmid, F.X. (1989). Cyclophilin and peptidyl-prolyl cis-trans isomerase are probably identical proteins. *Nature* 337, 476–478.
- Fregoso, O.I., Ahn, J., Wang, C., Mehrens, J., Skowronski, J., and Emerman, M. (2013). Evolutionary toggling of Vpx/Vpr specificity results in divergent recognition of the restriction factor SAMHD1. *PLoS Pathog.* 9, e1003496.
- Gamble, T.R., Vajdos, F.F., Yoo, S., Worthylake, D.K., Housewright, M., Sundquist, W.I., and Hill, C.P. (1996). Crystal structure of human cyclophilin A bound to the amino-terminal domain of HIV-1 capsid. *Cell* 87, 1285–1294.
- Greninger, A.L., Knudsen, G.M., Betegon, M., Burlingame, A.L., and Derisi, J.L. (2012). The 3A protein from multiple picornaviruses utilizes the golgi adaptor protein ACBD3 to recruit PI4KIIIβ. *J. Virol.* 86, 3605–3616.
- Gudmundsson, B., Jónsson, S.R., Olafsson, O., Agnarsdóttir, G., Matthiásdóttir, S., Georgsson, G., Torsteinsdóttir, S., Svansson, V., Kristbjörnsdóttir, H.B., Franzdóttir, S.R., et al. (2005). Simultaneous mutations in CA and Vif of Maedi-Visna virus cause attenuated replication in macrophages and reduced infectivity in vivo. *J. Virol.* 79, 15038–15042.
- Guo, Y., Dong, L., Qiu, X., Wang, Y., Zhang, B., Liu, H., Yu, Y., Zang, Y., Yang, M., and Huang, Z. (2014). Structural basis for hijacking CBF-β and CUL5 E3 ligase complex by HIV-1 Vif. *Nature* 505, 229–233.
- Han, X., Liang, W., Hua, D., Zhou, X., Du, J., Evans, S.L., Gao, Q., Wang, H., Viqueira, R., Wei, W., et al. (2014). Evolutionarily conserved requirement for core binding factor beta in the assembly of the human immunodeficiency virus/simian immunodeficiency virus Vif-cullin 5-RING E3 ubiquitin ligase. *J. Virol.* 88, 3320–3328.
- Harris, R.S., Bishop, K.N., Sheehy, A.M., Craig, H.M., Petersen-Mahrt, S.K., Watt, I.N., Neuberger, M.S., and Malim, M.H. (2003). DNA deamination mediates innate immunity to retroviral infection. *Cell* 113, 803–809.
- He, N., Liu, M., Hsu, J., Xue, Y., Chou, S., Burlingame, A., Krogan, N.J., Alber, T., and Zhou, Q. (2010). HIV-1 Tat and host AFF4 recruit two transcription elongation factors into a bifunctional complex for coordinated activation of HIV-1 transcription. *Mol. Cell* 38, 428–438.
- Huang, G., Shigesada, K., Ito, K., Wee, H.J., Yokomizo, T., and Ito, Y. (2001). Dimerization with PEBP2beta protects RUNX1/AML1 from ubiquitin-proteasome-mediated degradation. *EMBO J.* 20, 723–733.
- Hultquist, J.F., Lengyel, J.A., Refsland, E.W., LaRue, R.S., Lackey, L., Brown, W.L., and Harris, R.S. (2011). Human and rhesus APOBEC3D, APOBEC3F, APOBEC3G, and APOBEC3H demonstrate a conserved capacity to restrict Vif-deficient HIV-1. *J. Virol.* 85, 11220–11234.
- Hultquist, J.F., Binka, M., LaRue, R.S., Simon, V., and Harris, R.S. (2012). Vif proteins of human and simian immunodeficiency viruses require cellular CBFβ to degrade APOBEC3 restriction factors. *J. Virol.* 86, 2874–2877.
- Iwatani, Y., Chan, D.S.B., Wang, F., Maynard, K.S., Sugiura, W., Gronenborn, A.M., Rouzina, I., Williams, M.C., Musier-Forsyth, K., and Levin, J.G. (2007). Deaminase-independent inhibition of HIV-1 reverse transcription by APOBEC3G. *Nucleic Acids Res.* 35, 7096–7108.
- Jäger, S., Cimermančič, P., Gulbahce, N., Johnson, J.R., McGovern, K.E., Clarke, S.C., Shales, M., Mercenne, G., Pache, L., Li, K., et al. (2012a). Global landscape of HIV-human protein complexes. *Nature* 481, 365–370.
- Jäger, S., Kim, D.Y., Hultquist, J.F., Shindo, K., LaRue, R.S., Kwon, E., Li, M., Anderson, B.D., Yen, L., Stanley, D., et al. (2012b). Vif hijacks CBF-β to degrade APOBEC3G and promote HIV-1 infection. *Nature* 481, 371–375.
- Jarmuz, A., Chester, A., Bayliss, J., Gisbourne, J., Dunham, I., Scott, J., and Navaratnam, N. (2002). An anthropoid-specific locus of orphan C to U RNA-editing enzymes on chromosome 22. *Genomics* 79, 285–296.
- Jáuregui, P., Crespo, H., Glaria, I., Luján, L., Contreras, A., Rosati, S., de Andrés, D., Amorena, B., Towers, G.J., and Reina, R. (2012). Ovine TRIM5α can restrict visna/maedi virus. *J. Virol.* 86, 9504–9509.
- Jaya, N., Garcia, V., and Vierling, E. (2009). Substrate binding site flexibility of the small heat shock protein molecular chaperones. *Proc. Natl. Acad. Sci. USA* 106, 15604–15609.
- Katzourakis, A., Tristem, M., Pybus, O.G., and Gifford, R.J. (2007). Discovery and analysis of the first endogenous lentivirus. *Proc. Natl. Acad. Sci. USA* 104, 6261–6265.
- Kawakami, T., Sherman, L., Dahlberg, J., Gazit, A., Yaniv, A., Tronick, S.R., and Aaronson, S.A. (1987). Nucleotide sequence analysis of equine infectious anemia virus proviral DNA. *Virology* 158, 300–312.
- Kim, D.Y., Kwon, E., Hartley, P.D., Crosby, D.C., Mann, S., Krogan, N.J., and Gross, J.D. (2013). CBF-β stabilizes HIV Vif to counteract APOBEC3 at the expense of RUNX1 target gene expression. *Mol. Cell* 49, 632–644.

- Klase, Z., Yedavalli, V.S.R.K., Houzet, L., Perkins, M., Maldarelli, F., Brenchley, J., Strebel, K., Liu, P., and Jeang, K.-T. (2014). Activation of HIV-1 from latent infection via synergy of RUNX1 inhibitor Ro5-3335 and SAHA. *PLoS Pathog.* 10, e1003997.
- Lahaye, X., Satoh, T., Gentili, M., Cerboni, S., Conrad, C., Hurbain, I., El Marjou, A., Lacabaratz, C., Lelièvre, J.D., and Manel, N. (2013). The capsids of HIV-1 and HIV-2 determine immune detection of the viral cDNA by the innate sensor cGAS in dendritic cells. *Immunity* 39, 1132–1142.
- LaRue, R.S., Jónsson, S.R., Silverstein, K.A.T., Lajoie, M., Bertrand, D., El-Mabrouk, N., Hötzl, I., Andrésdóttir, V., Smith, T.P.L., and Harris, R.S. (2008). The artiodactyl APOBEC3 innate immune repertoire shows evidence for a multi-functional domain organization that existed in the ancestor of placental mammals. *BMC Mol. Biol.* 9, 104.
- Larue, R.S., Lengyel, J., Jónsson, S.R., Andrésdóttir, V., and Harris, R.S. (2010). Lentiviral Vif degrades the APOBEC3Z3/APOBEC3H protein of its mammalian host and is capable of cross-species activity. *J. Virol.* 84, 8193–8201.
- Lim, E.S., Fregoso, O.I., McCoy, C.O., Matsen, F.A., Malik, H.S., and Emerman, M. (2012). The ability of primate lentiviruses to degrade the monocyte restriction factor SAMHD1 preceded the birth of the viral accessory protein Vpx. *Cell Host Microbe* 11, 194–204.
- Löchelt, M., Romen, F., Bastone, P., Muckenfuss, H., Kirchner, N., Kim, Y.-B., Truyen, U., Rösler, U., Battenberg, M., Saib, A., et al. (2005). The antiretroviral activity of APOBEC3 is inhibited by the foamy virus accessory Bet protein. *Proc. Natl. Acad. Sci. USA* 102, 7982–7987.
- Luban, J., Bossolt, K.L., Franke, E.K., Kalpana, G.V., and Goff, S.P. (1993). Human immunodeficiency virus type 1 Gag protein binds to cyclophilins A and B. *Cell* 73, 1067–1078.
- Mangeat, B., Turelli, P., Caron, G., Friedli, M., Perrin, L., and Trono, D. (2003). Broad antiretroviral defence by human APOBEC3G through lethal editing of nascent reverse transcripts. *Nature* 424, 99–103.
- Miyagi, E., Kao, S., Yedavalli, V., and Strebel, K. (2014). CBF β enhances de novo protein biosynthesis of its binding partners HIV-1 Vif and RUNX1 and potentiates the Vif-induced degradation of APOBEC3G. *J. Virol.* 88, 4839–4852.
- Münk, C., Beck, T., Zielonka, J., Hotz-Wagenblatt, A., Chareza, S., Battenberg, M., Thielebein, J., Cichutek, K., Bravo, I.G., O'Brien, S.J., et al. (2008). Functions, structure, and read-through alternative splicing of feline APOBEC3 genes. *Genome Biol.* 9, R48.
- Nisole, S., Lynch, C., Stoye, J.P., and Yap, M.W. (2004). A Trim5-cyclophilin A fusion protein found in owl monkey kidney cells can restrict HIV-1. *Proc. Natl. Acad. Sci. USA* 101, 13324–13328.
- Ooms, M., Brayton, B., Letko, M., Maio, S.M., Pilcher, C.D., Hecht, F.M., Barbour, J.D., and Simon, V. (2013). HIV-1 Vif adaptation to human APOBEC3H haplotypes. *Cell Host Microbe* 14, 411–421.
- Ramage, H.R., Kumar, G.R., Verschueren, E., Johnson, J.R., Von Dollen, J., Johnson, T., Newton, B., Shah, P., Horner, J., Krogan, N.J., and Ott, M. (2015). A combined proteomics/genomics approach links hepatitis C virus infection with nonsense-mediated mRNA decay. *Mol. Cell* 57, 329–340.
- Rasaiyah, J., Tan, C.P., Fletcher, A.J., Price, A.J., Blondeau, C., Hilditch, L., Jacques, D.A., Selwood, D.L., James, L.C., Noursadeghi, M., and Towers, G.J. (2013). HIV-1 evades innate immune recognition through specific cofactor recruitment. *Nature* 503, 402–405.
- Roguev, A., Bandyopadhyay, S., Zofall, M., Zhang, K., Fischer, T., Collins, S.R., Qu, H., Shales, M., Park, H.O., Hayles, J., et al. (2008). Conservation and rewiring of functional modules revealed by an epistasis map in fission yeast. *Science* 322, 405–410.
- Ryan, C.J., Roguev, A., Patrick, K., Xu, J., Jahari, H., Tong, Z., Beltrao, P., Shales, M., Qu, H., Collins, S.R., et al. (2012). Hierarchical modularity and the evolution of genetic interactomes across species. *Mol. Cell* 46, 691–704.
- Sauter, D., Schindler, M., Specht, A., Landford, W.N., Münch, J., Kim, K.-A., Votteler, J., Schubert, U., Bibollet-Ruche, F., Keele, B.F., et al. (2009). Tetherin-driven adaptation of Vpu and Nef function and the evolution of pandemic and nonpandemic HIV-1 strains. *Cell Host Microbe* 6, 409–421.
- Sayah, D.M., Sokolskaja, E., Berthoux, L., and Luban, J. (2004). Cyclophilin A retrotransposition into TRIM5 explains owl monkey resistance to HIV-1. *Nature* 430, 569–573.
- Schwefel, D., Groom, H.C.T., Boucherit, V.C., Christodoulou, E., Walker, P.A., Stoye, J.P., Bishop, K.N., and Taylor, I.A. (2014). Structural basis of lentiviral subversion of a cellular protein degradation pathway. *Nature* 505, 234–238.
- Sharp, P.M., and Hahn, B.H. (2011). Origins of HIV and the AIDS pandemic. *Cold Spring Harb Perspect Med* 1, a006841.
- Sheehy, A.M., Gaddis, N.C., Choi, J.D., and Malim, M.H. (2002). Isolation of a human gene that inhibits HIV-1 infection and is suppressed by the viral Vif protein. *Nature* 418, 646–650.
- Sheehy, A.M., Gaddis, N.C., and Malim, M.H. (2003). The antiretroviral enzyme APOBEC3G is degraded by the proteasome in response to HIV-1 Vif. *Nat. Med.* 9, 1404–1407.
- Sokolskaja, E., and Luban, J. (2006). Cyclophilin, TRIM5, and innate immunity to HIV-1. *Curr. Opin. Microbiol.* 9, 404–408.
- Spiess, C., Miller, E.J., McClellan, A.J., and Frydman, J. (2006). Identification of the TRIC/CCT substrate binding sites uncovers the function of subunit diversity in eukaryotic chaperonins. *Mol. Cell* 24, 25–37.
- Stanley, D.J., Bartholomeeusen, K., Crosby, D.C., Kim, D.Y., Kwon, E., Yen, L., Cartozo, N.C., Li, M., Jäger, S., Mason-Herr, J., et al. (2012). Inhibition of a NEDD8 Cascade Restores Restriction of HIV by APOBEC3G. *PLoS Pathog.* 8, e1003085.
- Stremlau, M., Owens, C.M., Perron, M.J., Kiessling, M., Autissier, P., and Sodroski, J. (2004). The cytoplasmic body component TRIM5alpha restricts HIV-1 infection in Old World monkeys. *Nature* 427, 848–853.
- Tahirov, T.H., Inoue-Bungo, T., Morii, H., Fujikawa, A., Sasaki, M., Kimura, K., Shiina, M., Sato, K., Kumakura, T., Yamamoto, M., et al. (2001). Structural analyses of DNA recognition by the AML1/Runx-1 Runt domain and its allosteric control by CBFbeta. *Cell* 104, 755–767.
- Takahashi, N., Hayano, T., and Suzuki, M. (1989). Peptidyl-prolyl cis-trans isomerase is the cyclosporin A-binding protein cyclophilin. *Nature* 337, 473–475.
- Tan, M.J., White, E.A., Sowa, M.E., Harper, J.W., Aster, J.C., and Howley, P.M. (2012). Cutaneous β -human papillomavirus E6 proteins bind Mastermind-like coactivators and repress Notch signaling. *Proc. Natl. Acad. Sci. USA* 109, E1473–E1480.
- Thali, M., Bukovsky, A., Kondo, E., Rosenwirth, B., Walsh, C.T., Sodroski, J., and Göttlinger, H.G. (1994). Functional association of cyclophilin A with HIV-1 virions. *Nature* 372, 363–365.
- Thériault, Y., Logan, T.M., Meadows, R., Yu, L., Olejniczak, E.T., Holzman, T.F., Simmer, R.L., and Fesik, S.W. (1993). Solution structure of the cyclosporin A/cyclophilin complex by NMR. *Nature* 361, 88–91.
- White, E.A., Kramer, R.E., Tan, M.J., Hayes, S.D., Harper, J.W., and Howley, P.M. (2012a). Comprehensive analysis of host cellular interactions with human papillomavirus E6 proteins identifies new E6 binding partners and reflects viral diversity. *J. Virol.* 86, 13174–13186.
- White, E.A., Sowa, M.E., Tan, M.J., Jeudy, S., Hayes, S.D., Santha, S., Münger, K., Harper, J.W., and Howley, P.M. (2012b). Systematic identification of interactions between host cell proteins and E7 oncoproteins from diverse human papillomaviruses. *Proc. Natl. Acad. Sci. USA* 109, E260–E267.
- York, A., Hutchinson, E.C., and Fodor, E. (2014). Interactome analysis of the influenza A virus transcription/replication machinery identifies protein phosphatase 6 as a cellular factor required for efficient virus replication. *J. Virol.* 88, 13284–13299.

- Yu, X., Yu, Y., Liu, B., Luo, K., Kong, W., Mao, P., and Yu, X.F. (2003). Induction of APOBEC3G ubiquitination and degradation by an HIV-1 Vif-Cul5-SCF complex. *Science* **302**, 1056–1060.
- Zhang, H., Yang, B., Pomerantz, R.J., Zhang, C., Arunachalam, S.C., and Gao, L. (2003). The cytidine deaminase CEM15 induces hypermutation in newly synthesized HIV-1 DNA. *Nature* **424**, 94–98.
- Zhang, W., Du, J., Evans, S.L., Yu, Y., and Yu, X.-F. (2012). T-cell differentiation factor CBF- β regulates HIV-1 Vif-mediated evasion of host restriction. *Nature* **481**, 376–379.
- Zhang, J., Wu, J., Wang, W., Wu, H., Yu, B., Wang, J., Lv, M., Wang, X., Zhang, H., Kong, W., and Yu, X. (2014a). Role of cullin-elonginB-elonginC E3 complex in bovine immunodeficiency virus and maeedi-visna virus Vif-mediated degradation of host A3Z2-Z3 proteins. *Retrovirology* **11**, 77.
- Zhang, W., Wang, H., Li, Z., Liu, X., Liu, G., Harris, R.S., and Yu, X.-F. (2014b). Cellular requirements for BIV Vif-mediated inactivation of bovine APOBEC3 proteins. *J. Virol.*, Published online August 20, 2014 <http://dx.doi.org/10.1128/JVI.02072-14>.

Cell Reports

Supplemental Information

Lineage-Specific Viral Hijacking of Non-canonical E3 Ubiquitin Ligase Cofactors in the Evolution of Vif Anti-APOBEC3 Activity

Joshua R. Kane, David J. Stanley, Judd F. Hultquist, Jeffrey R. Johnson, Nicole Mietrach, Jennifer M. Binning, Stefán R. Jónsson, Sarah Barelier, Billy W. Newton, Tasha L. Johnson, Kathleen E. Franks-Skiba, Ming Li, William L. Brown, James S. Fraser, Reuben S. Harris, Valgerður Andrésdóttir, John D. Gross, and Nevan J. Krogan

1 **SUPPLEMENTAL INFORMATION**

2

3 **SUPPLEMENTAL EXPERIMENTAL PROCEDURES**

4

5 **Expression Constructs**

6 HIV-1_{LAI}, SIV_{mac239}, BIV, FIV, and MVV Vif constructs with C-terminal Myc tags in
7 pVR1012 (Vical Co.) have been reported previously (LaRue et al., 2010). All but
8 HIV-1_{LAI} sequence were subcloned into pcDNA4/TO expression vectors
9 (Invitrogen) using the restriction sites HindIII / Apal to match HIV-1_{NL4-3} Vif
10 plasmids used in previous affinity purification / mass spectrometry (AP-MS)
11 studies (Jäger et al., 2012a, 2012b). Human *APOBEC3G*, rhesus *APOBEC3G*,
12 cow *APOBEC3Z2Z3*, cat *APOBEC3Z2Z3*, and sheep *APOBEC3Z2Z3* constructs
13 with C-terminal 3xHA tags in pcDNA3.1(+) (Invitrogen) have been previously
14 reported (Hultquist et al., 2011; LaRue et al., 2008; Stenglein and Harris, 2006).
15 The CBFβ complementation construct in pcDNA3.1(+) has been previously
16 reported (Jäger et al., 2012b). CYPA was cloned from cDNA generated from
17 HEK293T cells and cloned into pcDNA4/TO vector. CAEV Vif and MVV Capsid
18 sequences were codon-optimized for human cell expression and synthesized
19 using gBlocks (IDT) from Uniprot entries P33462 and P35955 I144-363,
20 respectively, and subcloned into pcDNA4/TO 2xStrep vectors.

21

22 **Cell Lines**

23 Human Embryonic Kidney (HEK) 293T cells were maintained in high glucose
24 Dulbecco's Modified Eagle Medium (DMEM) containing 10% fetal bovine serum
25 (FBS), 2mM sodium pyruvate, and 1% penicillin/streptomycin (Pen/Strep). CBF β
26 knockdown HEK293T cells [reported previously (Jäger et al., 2012b)] were
27 maintained in identical conditions. CYPA knockdown 293T cells were maintained
28 in identical conditions, with 0.375 μ g / mL puromycin (Calbiochem) added to
29 maintain shRNA insert. CEM-GFP cells (obtained from the AIDS Research and
30 Reference Reagent Program) were maintained in RPMI with 10% FBS and 0.5%
31 Pen/Strep. Jurkat TRex cells (Invitrogen) were cultured in RPMI-1640 media,
32 10% FBS, 4 mM glutamine, 1% Pen/Strep, and 10 μ g / mL blasticidin (reported
33 previously (Jäger et al., 2012b)). Jurkat E6-1 and Jurkat CYPA $^{-/-}$ knockout cells
34 (obtained from the AIDS Research Reagent Program, #177 and #10095,
35 respectively) were maintained in RPMI-1640 media, 10% FBS, 4 mM glutamine,
36 and 1% Pen/Strep. Fetal lamb kidney (FLK) cells were cultured in DMEM high
37 glucose media, 10% FBS, and 1% Pen/Strep. Cell lines were maintained at 37°C
38 and 5% CO₂.

39

40 **Generation of Stable Jurkat TRex Vif Lines**

41 pcDNA4/TO Vif-3xFlag plasmids (MVV, BIV, FIV, SIVmac) were linearized by
42 digestion with Scal (NEB). 5x10⁶ Jurkat TRex cells were then electroporated with
43 20 μ g plasmid in 1 mL electroporation buffer (150 mM sucrose, 5 mM potassium
44 phosphate, 25 mM HEPES-KOH, 5 mM MgCl₂, 2 mM EDTA, 1% DMSO, 2 mM

45 MgATP, pH 7.4) in a 12-well electroporation plate with a GenePulser MXCell
46 (Bio-Rad) at 250V, 300 µF, and 1000 Ω. Cells were then placed under 300 µg /
47 mL Zeocin (Invitrogen) selection for 3 weeks, then subjected to limiting dilution to
48 generate monoclonal lines.

49

50 **Affinity Purifications**

51 Affinity purifications (AP) were generally performed as described previously
52 (Jäger et al., 2012a). For affinity purification, 4×10^6 cells were seeded in 15 cm
53 tissue culture plates and transfected the next day with 5 – 10 µg plasmid using
54 either calcium phosphate (Kingston et al., 2003) or Polyjet transfection reagent
55 (SignaGen). After approx. 42 hours post-transfection, cells were detached using
56 10 mM EDTA in PBS buffer and rinsed in cold PBS buffer. Stable Jurkat TRex
57 cells were grown in 250 mL media in spinner flasks. 2.5×10^8 cells were induced
58 with 1 µg / mL doxycycline for 16 hours prior to harvesting by centrifugation for
59 10 minutes at 4°C at 650 rpm, followed by rinsing in PBS. Cells were lysed in 1
60 mL cold lysis buffer [150 mM NaCl, 50 mM Tris-HCl, pH 7.4, 1 mM EDTA, 0.5%
61 NP40, protease inhibitor (cComplete-mini, Roche), phosphatase inhibitor
62 (phosSTOP, Roche)]. Cells were then either allowed to passively lyse on ice for
63 20 minutes or disrupted using ice-bath sonication, followed by lysate clearing at
64 2800 RCF for 30 minutes. Cells were then precleared with 70 µl agarose mouse
65 IgG beads (Sigma) for Flag APs, or 70 µl sepharose 4B beads (Sigma) for Strep
66 APs for 1 hour. Preclear lysates were then incubated with 35 µl M2 mouse anti-

67 Flag agarose beads (Sigma) for Flag IP or 35 µl StrepTactin beads (IBA) for
68 Strep AP; lysates and beads were rotated for 2 hours at 4°C. Beads were rinsed
69 3x times with wash buffer (150 mM NaCl, 50 mM Tris-HCl, pH 7.4, 1 mM EDTA,
70 0.05% NP40), followed by 1x rinse with wash buffer without detergent. Proteins
71 were eluted with 40 µl elution buffer [150 mM NaCl, 50 mM Tris-HCl, pH 7.4, 1
72 mM EDTA; for Flag elutions, 0.05% RapiGest (Waters) and 0.1 mg / mL 3xFlag
73 peptide (Elimbio); for Strep elutions, 2.5 mM D-desthiobiotin (IBA)]. 4 µl of the
74 eluate were analyzed by 4-20% SDS-PAGE (Bio-Rad) followed by silver stain
75 (Thermo).

76

77 **Immunoblotting**

78 6x sample buffer (Morganville Scientific, 9% 2-mercaptoethanol added fresh) was
79 added to samples prior to boiling for 5-10 minutes at 95°, and diluted with 1x
80 sample buffer if samples were concentrated or dilutions previously calculated by
81 BCA Assay (Thermo). SDS-PAGE was performed with denatured samples were
82 run on 4-12% NuPAGE gels in MOPS SDS running buffer (Invitrogen) at 170V for
83 approximately 1 hr. Samples were transferred to either PVDF or nitrocellulose
84 (Bio-Rad) in 48 mM Tris base, 39 mM glycine, 20% methanol at 100V for 60-90
85 minutes. Membranes were blocked in 5% BSA in TBS, 0.1% Tween-20 for 30
86 minutes. Immunoblotting was performed with the following antibodies: HA
87 (H3663, Sigma), Gapdh (#2118, CST), Strep (#34850, Qiagen), ELOB
88 (ab154854, Abcam), ELOC (#610760, BD Transduction Laboratories), CUL2

89 (A302-476A, Bethyl), CUL5 (A302-173A, Bethyl), Flag (F7425, A8592, Sigma),
90 CBFβ (sc-56751, SCBT), CYPA (ab41684, Abcam), GFP (kind gift of Dr. Andrew
91 A. Peden, University of Sheffield). Immunoreactive bands were detected either by
92 chemiluminescence (Pierce; Amersham) using anti-mouse or anti-rabbit
93 horseradish peroxidase (HRP) conjugated secondary antibodies (Bio-Rad), or
94 quantitatively by digital infrared scanner (LI-COR) using anti-mouse or anti-rabbit
95 fluorophore-conjugated secondary antibodies (LI-COR). Quantitative
96 immunoblotting bands were quantified using ImageJ software (Rasband, 2007).
97 For infectivity assays, cell lysates were prepared by resuspension of washed cell
98 pellets directly in 2.5x Laemmli Sample Buffer (32.5mM Tris pH 6.8, 10%
99 glycerol, 1.0% SDS, 2.5% 2-mercaptoethanol, 0.05% bromophenol blue), and
100 homogenization at 95°C for 30 minutes. Virus-like particles were isolated from
101 culture supernatants by purification through 0.45 µm PVDF filters (Millipore)
102 followed by centrifugation (13,000 rpm for 2 hours) through a 20% sucrose, 1x
103 PBS cushion and lysis directly in 2.5x Laemmli Sample Buffer. Samples were run
104 on 12.5% Tris-HCl SDS-PAGE resolving gels with 4% stacking gels each at a
105 37.5 acrylamide : 1 bis-acrylamide ratio (Bio-Rad Criterion) at 150V for 90
106 minutes. Proteins were transferred to PVDF membranes by methanol-based
107 electrotransfer (Bio-Rad Criterion Blotter) at 90V for 2 hours. Membranes were
108 blocked in 4% Milk in PBS, 0.1% Tween-20 overnight prior to overnight
109 incubation with primary antibody against HA to detect HA-tagged A3 (HA.11;
110 Covance), Myc to detect Myc-tagged Vif (9E10; Sigma), to detect CBFβ

111 complementation (T1832; Epitomics), TUB (tubulin; Covance), or p24/capsid
112 (NIH ARRRP 3537 courtesy of B. Chesebro and K. Wehrly). Anti-mouse and anti-
113 rabbit horseradish peroxidase (HRP)-conjugated secondary antibodies (Bio-Rad)
114 were detected using Hyglo HRP detection reagents (Denville Scientific). Blots
115 were incubated in a 1xPBS, 0.2M glycine, 1.0% SDS, 1.0% Tween-20, pH 2.2
116 stripping buffer before reprobing.

117

118 **Tandem Affinity Purification**

119 Four 15 cm plates per transfection were seeded with 4×10^6 HEK293T cells,
120 followed by a next day transfection of 5 – 10 μg plasmid per plate using Polyjet
121 transfection reagent (SigmaGen). 42 hours later, cells were harvested using 10
122 mM EDTA / PBS and pooled. Cells were pelleted at 400 RCF at 4°C for 5
123 minutes and resuspended by gentle pipetting in 6 mL lysis buffer [150 mM NaCl,
124 50 mM Tris-HCl, pH 7.4, 1 mM EDTA, 0.5% NP40, protease inhibitor (cOmplete-
125 mini, Roche), phosphatase inhibitor (phosSTOP, Roche)] and passively lysed by
126 rotating at 4°C for 20 minutes. Lysates were cleared with 2800 RCF, 45 minute,
127 4°C centrifugation. Cleared lysate was incubated with 120 μl StrepTactin beads
128 for 3 hours rotating at 4°C. Beads were washed 3x with wash buffer (150 mM
129 NaCl, 50 mM Tris-HCl, pH 7.4, 1 mM EDTA, 0.1% NP40), and eluted in 200 μl
130 Strep elution buffer [150 mM NaCl, 50 mM Tris-HCl, pH 7.4, 1 mM EDTA, 2.5 mM
131 D-desthiobiotin (IBA)] for 30 minutes at 4°C. Strep AP eluates were then
132 incubated with 20 μl M2 magnetic anti-Flag beads (Sigma) overnight. Flag beads

133 were washed 3x with wash buffer (described previously) and 2x in wash buffer
134 with no detergent. Proteins were eluted in 40 µl Flag elution buffer [150 mM
135 NaCl, 50 mM Tris-HCl, pH 7.4, 1 mM EDTA, 0.05% RapiGest (Waters) and 0.1
136 mg / mL 3xFlag peptide (Elimbio)]. Eluates were analyzed by immunoblotting and
137 mass spectrometry as described.

138

139 **Mass spectrometry analysis**

140 Purified proteins eluates were digested with trypsin for LC-MS/MS analysis.
141 Samples were denatured and reduced in 2M urea, 10 mM NH₄HCO₃, 2 mM DTT
142 for 30 minutes at 60°C, then alkylated with 2 mM iodoacetamide for 45 at room
143 temperature. Trypsin (Promega) was added at a 1:100 enzyme:substrate ratio
144 and digested overnight at 37°C. Following digestion, samples were concentrated
145 using C18 ZipTips (Millipore) according to the manufacturer's
146 specifications. Digested peptide mixtures were analyzed by LC-MS/MS on either
147 a Thermo Scientific Velos Pro or a Thermo Scientific LTQ XL ion trap mass
148 spectrometry system equipped with a Proxeon Easy nLC high pressure liquid
149 chromatography and autosampler system. Samples were injected onto a pre-
150 column (2 cm x 100 um I.D. packed with ReproSil Pur C18 AQ 5um particles) in
151 0.1% formic acid and then separated with a two-hour gradient from 5% to 30%
152 ACN in 0.1% formic acid on an analytical column (10 cm x 75 um I.D. packed
153 with ReproSil Pur C18 AQ 3 um particles). The mass spectrometer collected data
154 in a data-dependent fashion, collecting one full scan followed by 20 collision-

155 induced dissociation MS/MS scans of the 20 most intense peaks from the full
156 scan. Dynamic exclusion was enabled for 30 seconds with a repeat count of 1.
157 The results raw data was matched to protein sequences by the Protein
158 Prospector algorithm. Data were searched against a database containing
159 SwissProt Human protein sequences (downloaded March 6, 2012) and lentivirus
160 sequences, concatenated to a decoy database where each sequence was
161 randomized in order to estimate the false positive rate. The searches considered
162 a precursor mass tolerance of 1 Da and fragment ion tolerances of 0.8 Da, and
163 considered variable modifications for protein N-terminal acetylation, protein N-
164 terminal acetylation and oxidation, glutamine to pyroglutamate conversion for
165 peptide N-terminal glutamine residues, protein N-terminal methionine loss,
166 protein N-terminal acetylation and methionine loss, and methionine oxidation,
167 and constant modification for carbamidomethyl cysteine. Prospector data was
168 filtered using a maximum protein expectation value of 0.01 and a maximum
169 peptide expectation value of 0.05.

170

171 **Mass Spectrometry Data Analysis**

172 Interactions were scored using the SAINT algorithm (Choi et al., 2011) with prey
173 identified spectral counts, using empty vector and HIV-1 Nef transfections as
174 negative controls; for Jurkat T-cell data, reference Jurkat cells AP-MS results
175 were also included. A threshold SAINT probability ≥ 0.9 for at least one bait-prey
176 interaction was set the cut-off for prey inclusion in the final dataset. Data was

177 hierarchically clustered by correlation using the Cluster3 program (de Hoon et al.,
178 2004) and visualized using the Java TreeView program (Saldanha, 2004).

179

180 **HIV-1 Single Cycle Assay with Replication Proficient Virus**

181 At 50% confluency, CBF β knockdown HEK293T cells were transfected (TransIt,
182 Mirus) with 1 mg Vif-deficient ($X_{26}X_{27}$) HIV-1_{IIIB} A200C proviral construct (Haché
183 et al., 2008) in the presence or absence of 50 ng of the indicated C-terminal HA-
184 tagged A3 expression construct, 25 ng of the species cognate C-terminal Myc-
185 tagged Vif expression construct, and 50 ng untagged human CBF β . After 48
186 hours to allow for virus production, portions of the virus-containing supernatants
187 were used to infect 25,000 CEM-GFP cells in 96-well plates to titer. The rest of
188 the viral supernatant and the cells were processed for immunoblotting. After
189 another 48 hours, the CEM-GFP cells were fixed in 4% paraformaldehyde and
190 GFP positive cells quantified by flow cytometry (see below). Data was normalized
191 to the no A3, no Vif, no CBF β control for each species as 100% infectivity.

192

193 **Flow Cytometry**

194 HIV-1 -infected CEM-GFP cells were prepared for flow cytometry by fixation in
195 4% paraformaldehyde, 1x PBS. GFP fluorescence was measured on a Becton
196 Dickinson FACS Canto II flow cytometer. All data was analyzed using FlowJo
197 Flow Cytometry Analysis Software (Version 8.8.6). Quantification was done by
198 first gating the live cell population, followed by gating on the GFP $^{+}$ cells.

199

200 **Vif Site-Directed Mutagenesis**

201 BC-mutant proteins were generated using site-directed mutagenesis via a quick-
202 change PCR (QC-PCR) protocol. pcDNA4/TO Vif-2xStrepII plasmids were
203 amplified using PfuUltra (Agilent) and primers targeting Vif BC-box S/TLQ motifs
204 (Suppl. Figure 1B). Products were DpnI (NEB) digested then transformed into
205 Top10 cells (Invitrogen). The following primers were used:

Primer	Sequence (5'-to-3')
mvv-vif-qc-slq-fw	TAACCCCAGAGCCGCGGCGAGACTTGCCCTGCTTCACCTCG
mvv-vif-qc-slq-rv	GGGCAAGTCTGCCGCGGCTCTGGGGTTAGTGTAAAAAAGAC
biv-vif-qc-slq-fw	CCCACGCCACGCCGCGCGCAGCTGGCAGCTCTGCAGCTC
biv-vif-qc-slq-rv	CTGCCAGCCGCCGCCGCGCTGGCGTGGCTGGGTAGAGGTCAG
fiv-vif-qc-tlq-fw	CCCACCACAGGCCGCCGCCGCGCTGGCCATGCTGGCTTG
fiv-vif-qc-tlq-rv	TGGCCAGCCGCCGCCGCCGCTGTGGTGGCTGTTCCGCAG
siv-vif-qc-slq-fw	CCAGGTTCCCTGCTGCCGCGTATCTGGCACTCAAAGTCGTTTC
siv-vif-qc-slq-rv	GTGCCAGATAGCCGCCAGCAGGAACCTGGTACTTGTGAGC
hiv-qc-slq-fw	CAAGGTCGGGGCCGCCGCGTATCTGGCACTGGCAGCCCTG
hiv-qc-slq-rv	GTGCCAGATAGCCGCCGCCGACCTTGTGGCCGGC

206 For MVV Vif proline-to-alanine mutants, the same QC-PCR protocol was used
207 with the pcDNA4/TO MVV Vif-2xStrep template with following primers:

Primer	Sequence (5'-to-3')
mvv-vif-P21A-P24A-fw	GGAGATAGGCAGCCAGCTGGCACTGTGGCATGGAAAGAAC
mvv-vif-P21A-P24A-rv	ATGCCACAGTGCCAGCTGGCGCCTATCTCCGGCCTGTT
mvv-vif-P171A-fw	AAACACTAACGCCAGAACGCTGCAGAGACTTGC

mvv-vif-P171A-rv	GCAGGCTTCTGGCGTTAGTGTAAAAACATC
mvv-vif-P216A-fw	ATACACCATGCCTGGAGTCTGCAGGAGTGTG
mvv-vif-P216A-rv	GCAGACTCCAGGCGATGGTGTATCCCATTGGAG
mvv-vif-P21A-fw	GGAGATAGGCGCCCAGCTGCCACTGTGGGCATGGAAAGAAC
mvv-vif-P21A-rv	ATGCCACAGTGGCAGCTGGCGCCTATCTCCCGGGCCTGTTC
mvv-vif-P24A-fw	GGAGATAGGCCCCCAGCTGGCACTGTGGGCATGGAAAGAAC
mvv-vif-P24A-rv	ATGCCACAGTGCCAGCTGGGGCCTATCTCCCGGGCCTGTTC
mvv-vif-P39A-fw	CAATCAGGAGGCCTACTGGTATAGCACTATTAGAC
mvv-vif-P39A-rv	TATACCAGTAGGCCTCCTGATTGATAGAGAATGCTG
mvv-vif-P116A-fw	GTACGAGAGCGCCGGAGACTACAAGGGAAAAGAG
mvv-vif-P116A-rv	TGTAGTCTCCGGCGCTCTCGTACCAACACCCATTG
mvv-vif-P192A-fw	CCAGGTCATGGCTTTGGAGGGCACGGAGGGTG
mvv-vif-P192A-rv	CCCTCCAAAGAGCCATGACCTGGAACACATGATC
mvv-vif-P205A-fw	GCAAAAGTCGCATGGTCAGGTCTCCAATGGGATAC
mvv-vif-P205A-rv	ACCTGCACCATGCGAACTTTGCACAGTCACCCCTC
mvv-vif-P210A-fw	GTGCAGGTCTGCAATGGGATACACCATCCCTGGAG
mvv-vif-P210A-rv	TGTATCCCATTGCAGACCTGCACCATGGGAACTTTG

208

209 **Generation of CYPA Mutants**

210 Following the same protocol as with Vif site-directed mutagenesis, we generated
 211 CYPA active-site point mutants R55K, F113W, and H126A using the following
 212 primers:

Primer	Sequence (5'-to-3')
CYPA-R55K-fw	GTTCCCTGCTTCACAAAATTATTCCAGGGTTATGTGTC
CYPA-R55K-rv	CCCTGGAATAATTTGTGAAAGCAGGAACCCTATAAC

CYPA-F113W/fw	GGTCCCAGTTTGGATCTGCACTGCCAAGACTGAGTG
CYPA-F113W-rv	CTTGGCAGTGCAGATCCAAAATGGAACCATTTGTGTTGG G
CYPA-H126A-fw	GTTGGATGGCAAGGCTGTGGTGGCAAAGTGAAAGAAG
CYPA-H126-rv	CTTGCCAAACACCACAGCCTGCCATCCAACCACTCAGTCT TG

213

214 To generate shRNA resistant constructs in order to perform rescue experiments
 215 in CYPA knockdown background, we targeted the region in CYPA CDS targeted
 216 by the shRNA used in the monoclonal knockdown line (#49277; 349-
 217 GCCAAGACTGAGTGGTTGGAT-369). The following primers were used:

Primer	Sequence (5'-to-3')
CYPA wt+R55K sh-resist-fw	CATCTGCACTGCGAAAACAGAATGGCTCGACGGCAAGCATG TGGTGTGG
CYPA wt+R55K sh-resist-rv	ACATGCTTGCCGTCGAGCCATTCTGTTTCGCAGTGCAGAT GAAAAACTG
CYPA F113W sh-resist-fw	CATCTGCACTGCGAAAACAGAATGGCTCGACGGCAAGCATG TGGTGTGG
CYPA F113W sh-resist-rv	ACATGCTTGCCGTCGAGCCATTCTGTTTCGCAGTGCAGAT CCAAAAACTG
CYPA H126A sh-resist-fw	CATCTGCACTGCGAAAACAGAATGGCTCGACGGCAAGGCTG TGGTGTGG
CYPA H126A sh-resist-rv	ACAGCCTTGCCGTCGAGCCATTCTGTTTCGCAGTGCAGAT GAAAAACTG

218

219 **Generation of CYPA Knockdown Lines**

220 Lentiviruses were generated using HEK293T cells. Cells were transfected in 6-
221 well format with pCMV-VSV-G, pCMV-dR8.91, and pLKO.1 lentivirus vector
222 using Polyjet transfection reagent (SigmaGen). Lentiviruses were titered,
223 polybrene added to increase transduction efficiency, and HEK293T cells were
224 transduced with lentiviruses expressing either an shRNA against CYPA
225 (TRCN0000049271; TRCN0000049277) or a scrambled control (SHC002;
226 Sigma), and subjected to puromycin selection. Verification of knockdown was
227 assessed by immunoblotting. A monoclonal line was generated from the
228 TRCN0000049277 transduced cells by limiting dilution.

229

230 **CYPA Co-Immunoprecipitation Assays**

231 5×10^6 cells were seeded in 6-well plates and transfected the following day with
232 0.5 μ g CYPA-3xFlag and 1 μ g MVV Vif-2xStrepII constructs. 42 hours post-
233 transfection, cells were harvested and Strep AP performed as described above
234 using 10 μ l StrepTactin beads and a 2 hour incubation at 4°C, eluting in 20 μ l
235 Strep elution buffer [150 mM NaCl, 50 mM Tris-HCl, pH 7.4, 1 mM EDTA, 2.5 mM
236 D-desthiobiotin (IBA)].

237

238 **Cyclosporine A Affinity Purification Assays**

239 Approximately 5×10^6 HEK293T cells were seeded in 15 cm plates, and
240 transfected the next day with 7.5 μ g MVV Vif-2xStrepII constructs or a vector

241 control using calcium phosphate precipitation. 4-6 hours post-transfection, media
242 was replaced with fresh media containing either ethanol or appropriate
243 concentration of cyclosporine A (CsA) (#9973, CST). 24 hours post-transfection,
244 cells were harvested and Strep AP performed as described, with ethanol or CsA
245 was added to lysis buffer of appropriate samples to prevent washing out of CsA
246 and re-association of MVV Vif-CYPA complexes *ex vivo*.

247

248 **Cyclosporine A – A3 Degradation Assays**

249 2.5x10⁵ HEK293T cells were seeded in 12-well plates and transfected the
250 following day with 200 ng of pcDNA3.1-OaA3Z2Z3-3xHA and 100 ng
251 pcDNA4/TO-MVV-Vif-2xStrep constructs using Polyjet transfection reagent
252 (SigmaGen); for control experiments, 200 ng pcDNA3.1-Hs-A3G-3xHA and 20 ng
253 pcDNA4/TO-HIV1-Vif-2xStrep constructs were used. 6 hours post-transfection,
254 cells were treated with cyclosporine A (#9973, CST) or ethanol. 25 hours post-
255 transfection, cells were harvested and lysed in RIPA buffer [150 mM NaCl, 50
256 mM Tris-HCl pH 7.4, 1 mM EDTA, 1% NP40, 0.5% sodium deoxycholate, 0.1%
257 SDS, protease inhibitor (cOmplete-mini, Roche), phosphatase inhibitor
258 (phosSTOP, Roche)]. Cells were lysed for 20 minutes on ice followed by 20,000
259 RCF, 4°C, 5 minutes lysate clearing. Prior to adding 6x sample buffer, a BCA
260 assay (Thermo) was performed to calculate protein concentration using a bovine
261 serum albumin standard. Supernatant was boiled in sample buffer and 4-12%
262 SDS-PAGE (Invitrogen) was performed loading approx. 4 µg of protein per

263 sample, followed by transfer to nitrocellulose membrane (Bio-Rad). HA
264 immunoreactivity bands were measured quantitatively by digital infrared scanner
265 (LI-COR), then normalized by GAPDH, and these values were normalized to no
266 Vif controls for each line (A3-3xHA alone). Additional immunop probing of
267 membranes (Strep, CYPA) were developed by chemiluminescence.

268

269 **Jurkat Nucleofections**

270 Jurkat E6-1 and *CYPA*^{-/-} knockout lines were transfected using the Lonza
271 nucleofection kit (Cell Line Nucleofector V, Lonza) and following their Jurkat
272 optimized protocol (X-005). Briefly, 1x10⁶ Jurkat cells were pelleted at 500 rpm
273 for 10 minutes at room temperature, then resuspended in nucleofection reagent.
274 2 µg of DNA was then added to the resuspended cells, and cells were
275 nucleofected using the X-005 protocol, incubated with DNA and reagent for 10
276 minutes, and resuspended in 0.5 mL pre-warmed media and added to 12-well
277 plate well containing 1 mL pre-warmed media. Cells were harvested
278 approximately 40 hours post-nucleofection.

279

280 **Jurkat CYPA Knockout A3 Degradation and Rescue Assays**

281 Jurkat E6-1 or *CYPA*^{-/-} knockout lines were transfected with 1 µg OaA3Z2Z3-
282 3xHA, HsA3G-3xHA, or vector; 0.4 µg MVV Vif-2xStrep, 0.2 µg HIV-1 Vif-
283 2xStrep, or vector; 0.5 µg CYPA-3xFlag or vector; 0.1 µg eGFP; and vector to
284 total 2 µg per nucleofection. Cells were harvested approximately 40 hours post-

285 nucleofection, pelleted at 400 RCF for 10 minutes at room temperature, and
286 lysed in 50 µl 1x sample buffer (Morganville Scientific) and boiled for 30 minutes
287 prior to SDS-PAGE and subsequent immunoblotting. CYPA rescue experiments
288 were performed with 0.5 µg of either wild-type, R55K, F113W, or H126A CYPA-
289 3xFlag; mutants were generated as described previously.

290

291 **CYPA Monoclonal Knockdown Rescue Assay**

292 2×10^5 monoclonal CYPA knockdown line (shRNA TRCN0000049277) in 293T
293 background cells were seeded per well in a 12-well plate (Costar). 24 hours later,
294 cells were transfected with 200 ng OaA3Z2Z3-3xHA plasmid or vector; 25 ng
295 MVV Vif-2xStrep or vector; and 250 ng wild-type, R55K, F113W, or H126A
296 shRNA-resistant CYPA-3xFlag or vector using Polyjet transfection reagent
297 (SignaGen). Cells were harvested 24 hours later, lysed in RIPA buffer (150 mM
298 NaCl, 50 mM Tris-HCl, pH 7.4, 1 mM EDTA, 1% NP40, 0.5% Sodium
299 Deoxycholate, 0.1% SDS), and lysates subjected to SDS-PAGE.

300

301 **Recombinant Protein Expression Vectors**

302 Cow and sheep A3Z3 genes have been described (Jónsson et al., 2006; LaRue
303 et al., 2008, 2010). The cDNA were PCR amplified with following primers: cow
304 A3Z3, forward 5'- nnnnGAATTCGCCACCATGACCGAGGGCTGG -3', reverse 5'-
305 nnnnAAGCTT AATTGGGGCCGTTAG-3'; sheep A3Z3, forward 5'-
306 nnnnGAATTCGCCACCATGACGGAGGGCTGG-3', reverse 5'-

307 nnnnAAGCTTAGTCGGCGCCGTCAG-3'. The PCR products were digested with
308 EcoRI and HindIII, gel-purified and inserted into eukaryotic expression vector
309 pcDNA3.1-Myc-His (Invitrogen) digested with the same enzymes.

310

311 **A3 Protein Purification**

312 A3Z3-Myc-His proteins were purified with previously described protocol (Li et al.,
313 2012; Nowarski et al., 2008; Stenglein et al., 2010). Briefly, 1×10^8 of HEK-293T
314 cells transiently transfected with pcDNA3.1-BtA3Z3-myc-His or pcDNA3.1-
315 OaA3Z3-Myc-His were harvested, washed with PBS and resuspended in 10ml of
316 cell lysis buffer (25mM HEPES, pH7.4, 150mM NaCl, 0.5% Triton X-100, 1mM
317 EDTA, 1mM MgCl₂, 1mM ZnCl₂, 10% Glycerol, Roche EDTA-free complete
318 protease inhibitor cocktail) supplemented with 50 µg/ml RNase A (Qiagen). The
319 cell suspension was incubated on ice for 1 hour with periodic vortexing, followed
320 by incubation at 25°C for 20 min. The lysates were then clarified by centrifugation
321 (12,000g, 4°C, 10 min). NaCl was added to the lysates to bring the final
322 concentration to 0.8 M. The lysates were then mixed with 50 µl Ni-NTA agarose
323 (Qiagen) by rotating over night at 4°C. The suspension was then loaded onto a
324 Poly-Prep chromatography column (Bio-Rad). Following extensive washing with
325 wash buffer (50 mM Tris, pH 8.0, 0.3 M NaCl, 10% glycerol, 0.5% Triton X-100,
326 50 mM imidazole), each A3-Myc-His protein was eluted with elution buffer (50
327 mM Tris, pH 8.0, 0.3 M NaCl, 10% glycerol, 0.5% Triton X-100, 250 mM
328 imidazole). Protein purity was assessed by SDS-PAGE and Coomassie blue

329 R250 staining. Protein concentration was determined by densitometry compared
330 to bovine serum albumin standards and by the Bradford assay (Bio-Rad).

331

332 **Cullin Ligase Protein Expression and Purification**

333 Vif complexes for *in vitro* work were produced by coexpression in BL21-
334 Star(DE3)pLysS cells. For trimers (Vif-ELOB-ELOC), Vif was expressed from a
335 pET28a-derived vector as a fusion protein with an N-terminal 6xHis-GST tag. For
336 tetramers (Vif-CYPA/CBF β -ELOB-ELOC), a pETDuet vector was used that
337 encoded both untagged Vif and either CYPA or CBF β as a fusion protein with an
338 N-terminal 6xHis-TRX tag. All tags were removed by cleavage with TEV protease
339 as a purification step. A previously described pCDFDuet vector encoding both
340 ElonginB and ElonginC was used in all cases (Kim et. al 2013). All protein
341 expression was induced at OD~1.0 at a temperature of 16°C, and allowed to
342 proceed for 15-18 hours. Cells were harvested by centrifugation, and washed
343 once with 1X PBS. Washed cell pellets were immediately flash frozen and stored
344 at -20°C. Cells were resuspended in roughly 20 mL lysis buffer (25 mM HEPES
345 pH 7.5, 0.5 M NaCl, 5% glycerol, 20 mM imidazole, 2mM DTT) per liter of cell
346 culture, and lysed by sonication. Cell debris was pelleted by centrifugation at
347 16,000 RCF for 40 minutes, and the resulting supernatant was loaded onto a 5
348 mL NiNTA HisTrap column (GE Healthcare). Following extensive washing with
349 lysis buffer, bound proteins were eluted by an imidazole gradient. At this stage
350 fusion tags were removed by incubation with TEV protease, and further purified

351 by a combination of heparin affinity and/or size exclusion chromatography. A
352 notable exception was the purification of the MVV Vif tetrameric complex, in
353 which heparin affinity chromatography was performed immediately after the
354 NiNTA step, in order to isolate tetrameric complex from the large excess of free
355 TRX-CYPA. E3 ligase complexes were assembled by mixing an excess of Vif
356 subcomplexes with CUL5-RBX2, followed by size exclusion chromatography to
357 isolate the resultant pentamer or hexamer. All purifications were finished by size
358 exclusion chromatography into a final buffer of 25 mM HEPES pH 7.5, 0.3 M
359 NaCl, 5% glycerol, 2mM DTT. CUL5-RBX2, and all ubiquitin and Nedd8 pathway
360 components used in ubiquitylation assays were obtained as previously described
361 (Stanley et al., 2012).

362

363 ***In vitro* ubiquitylation assays**

364 Assays for ubiquitylation activity of reconstituted Vif E3 ligases were initiated out
365 by mixing together separate NEDD8-charging and ubiquitin-charging reactions
366 with myc-tagged A3 substrate. Prior to mixing, the charging reactions were
367 incubated at room temperature for 30 minutes to fully charge E2 enzymes and
368 fully NEDD8ylate E3s. This final mixture contained the following components in a
369 buffer of 25 mM HEPES pH 7.5, 50 mM NaCl, 2.5 mM MgCl₂: 50 nM NAE1, 5
370 μM UBE2F, 12.5 μM NEDD8, 300 nM Vif E3, 50 nM UBE1, 5 μM UBE2R1, 12.5
371 μM UBIQUITIN, 2 mM ATP, 1 mg/mL BSA. The reaction was allowed to
372 incubate at room temperature for 2 hours, and stopped with SDS-PAGE loading

373 dye and heat denaturation. Reaction products were visualized by immunoblotting
374 with an anti-c-Myc mAb (M4439, Sigma).

375

376 **Small-angle X-ray Scattering**

377 Samples for small-angle X-ray scattering (SAXS) were dialyzed extensively
378 against 20 mM Tris-HCl (pH 8.0), 500 mM NaCl, 10% (w/v) glycerol, and 2 mM
379 TCEP, and filtered through 0.1 µm membranes (Millipore, Bedford, MA) prior to
380 data collection. SAXS profiles of HIV-1 E3 and MVV E3 were measured at
381 concentrations of 0.5, 1.0, 1.5, 2.0, and 4.4 mg/ml at 10°C, using up to 15, 1
382 second exposures at Beamline 4-2 of the Stanford Synchrotron Radiation
383 Lightsource (SSRL) in the SLAC National Accelerator Laboratory (Menlo Park,
384 CA). The buffer profile was obtained in the same manner and subtracted from a
385 protein profile. The merged scattering profiles were processed using software in
386 the ATSAS package (Konarev et al., 2006). 20 independent *ab initio* envelopes
387 were generated using DAMMIF (Franke and Svergun, 2009) and consensus
388 models were obtained using DAMAVER (Volkov and Svergun, 2003). The
389 DAMAVER output was refined against using DAMMIN (Svergun, 1999). The final
390 NSD values for the HIV-1 E3 and MVV E3 envelopes were 0.679 and 0.820,
391 respectively. All plots were generated using ORIGIN 8.0 (OriginLab,
392 Northampton, MA), and final SAXS envelopes were draw in Chimera (Pettersen
393 et al., 2004). The HIV E3 atomic resolution model used to fit the SAXS envelopes
394 was constructed based on the HIV-1 Vif, CBFβ, ELOB, ELOC, CUL5 N-terminal

395 crystal structure (PDB ID: 4N9F). The full-length CUL5 model was generated
396 using MODELER (Sali and Blundell, 1993) with HIV-1 Vif complex (PDB
397 ID:4N9F), CUL5 CTD (PDB ID: 2WZK), and full-length Cullin-1 and Cullin-4 (PDB
398 IDs: 1LDJ and 2HYE). The HIV-1 E3 model was further refined using the
399 AllosMod-FoXS server (<http://salilab.org/allosmod>) (Schneidman-Duhovny et al.,
400 2010; Weinkam et al., 2012) to obtain a model which fit our experimental SAXS
401 profile with a Chi value of 1.89.

402

403 **Informatics**

404 Percent identity / similarity matrix for Vif proteins used in this study was
405 generated using by the EMBOSS tool Needle (Rice et al., 2000) using the
406 following settings – Gap-open: 8.0, Gap-extend: 0.5, End-open: 10.0, End-
407 extend: 0.5, Matrix: Blosum45. Multiple sequence alignment of Vif sequences
408 was performed using the PSI-Coffee variant of the T-Coffee alignment algorithm
409 (Notredame et al., 2000) and visualized using JalView (Waterhouse et al., 2009).
410 Lentivirus Gagpol tree was generated from the sequence entries in Uniprot
411 (P05897, P12497, P16087, P16088, P19560, P35955, P35956). Sequences
412 were aligned using PSI-Coffee, curated using Gblocks (Castresana, 2000) on
413 *Phylogeny.fr* (Dereeper et al., 2008), and a maximum likelihood tree with
414 bootstrap values generated using the RAxML Blackbox (Stamatakis et al., 2008).
415 Statistics on MVV KV1772 hypermutation was performed using the statistical

416 software package R (R Core Team, 2014) using a one-sided Wilcoxon Ranked-
417 Sum test.

418

419 **Construction of mutant viruses**

420 The MVV molecular clone KV1772 is split between two plasmids, p8XSp5-RK1
421 and p67r, as has been described previously (Skraban et al., 1999). For
422 construction of the single mutants Vif P21A and Vif P24A and the double mutant
423 Vif P21A/P24A, a subclone of p8XSp5-RK1 containing nucleotides 4587-6392
424 was used for PCR-based mutagenesis. Briefly, complementary oligos containing
425 the respective mutations were used for amplification. The PCR products were
426 treated with DpnI to degrade parental DNA, and transformed into E. coli. The
427 resulting plasmids were cleaved with MluI and BglII and the MluI₄₆₈₀ - BglII₅₈₄₁
428 fragment was isolated and exchanged for the equivalent fragment in p8XSp5-
429 RK1. All constructs were verified by DNA sequencing.

430 For transfections, equimolar quantities of the two plasmids containing the viral
431 genome, a total of 6 µg, were cut with XbaI and ligated. Transfections of primary
432 sheep choroid plexus (SCP) cells were carried out using Lipofectamine 2000 in
433 T25 tissue culture flasks as specified by the manufacturer (Invitrogen).
434 Supernatants were clarified by centrifugation at 3000 rpm for 3 min. and kept at -
435 80°C.

436

437 **Ovine cells and MVV infections**

438 Primary sheep choroid plexus (SCP) cells were cultured in Dulbecco's modified
439 Eagle's medium supplemented with antibiotics and 10% and 1% lamb serum for
440 growth and maintenance respectively. Sheep blood-derived macrophage cultures
441 were established as described previously (Skraban et al 1999). SCP cells and
442 sheep blood-derived macrophages were infected with RT-normalized wild-type
443 and mutant viruses for spreading infection assays. 500 µl samples were taken
444 every day for Taqman qPCR analysis and replaced by the same volume of fresh
445 medium.

446

447 **RT assay**

448 Viral particles from 200 µl of cell-free supernatants from infected cells were
449 pelleted at 14,000 rpm for 1 hour in a microfuge. The pelleted virus was
450 resuspended in TNE (10mM Tris-HCl (pH7.5), 100 mM NaCl, 1 mM EDTA)
451 containing 0.1% Triton X-100. RT activity was assayed on a poly (A) template,
452 adding oligo-dT primer and dTTP. The resulting RNA-DNA heteroduplexes were
453 detected by PicoGreen reagent as specified by the manufacturer (Molecular
454 Probes Inc., Eugene, Oregon).

455

456 **MVV Genome Copy Quantification**

457 Viral particles from 200 µl cell-free supernatants from infected cells were pelleted
458 at 14,000 rpm for 1 hour in a microfuge. The pellet was dissolved in 10 µl TNE
459 (10 mM Tris pH 7.5; 100 mM NaCl; 1 mM EDTA) with 0.1% Triton X-100. This

460 lysate was used for generating cDNA using MultiScribe reverse transcriptase
461 (Applied Biosystems) and a primer from the gag gene (V-1818; 5'-
462 CGGGGTACCTAACACATAGGGGGCGCGG-3'). Real-time PCR was carried
463 out in a final volume of 20 µl. The primers and Taqman probe were as follows:
464 Forward primer: V1636; 5'-TAAATCAAAAGTGTATAATTGTGGGA-3', reverse
465 primer: V-1719; 5'-TCCCACAATGATGGCATATTATTC-3', Taqman probe: V1665
466 Taqman; 5'-FAM-CCAGGACATCTCGCAAGACAGTGTAGACA-BHQ-1-3'.
467 Calibration curves were derived by running 10-fold dilutions of specific cDNA
468 over the range of 6x10 - 6x10⁷ copies. Each assay included triplicate wells for
469 each dilution of calibration DNA and for each cDNA sample.

470

471 **MVV Proviral DNA sequence analysis**

472 Genomic DNA was prepared from MVV infected SCP cells using the Gentra
473 Puregene Cell Kit (Qiagen). A 1034 bp fragment from the *env* gene (nt 6911-
474 7945) of integrated proviruses was amplified using Phusion DNA polymerase and
475 treated with Taq DNA polymerase before being cloned into TOPO-TA vectors
476 (Invitrogen). Ten to twenty clones were sequenced for each virus strain.
477 Sequences were analyzed using Sequencher, version 5.0 (Genes Codes Corp.).

478

479 **NMR**

480 NMR spectra were recorded at 10°C on a Bruker 800 MHz equipped with a
481 cryogenic probe. A 440 µM sample was prepared in 50 mM phosphate buffer pH

482 7.0, 10% D₂O. ¹H–¹⁵N HSQC spectra were recorded on CYPA, in presence of
483 increasing amounts of MVV Vif peptide (17-REIGPQLPLW-26) (from 0 to 300
484 μM, adding 25 μM at a time). All NMR spectra were processed with Topspin3
485 (Bruker) and analyzed with the CCPN suite (Vranken et al., 2005).

486

487

488 **SUPPLEMENTAL FIGURE LEGENDS**

489

490 **Figure S1. Multiple Sequence Alignment of Lentivirus Vif Proteins. Related**
491 **to Figure 1**

492 (A) Multiple sequence alignment of Vif proteins used in this study. Alignment was
493 performed by the PSI-Coffee variant of the T-Coffee alignment algorithm
494 (Notredame et al., 2000). Residues were highlighted by BLOSUM62 similarity
495 using the software Jalview (Waterhouse et al., 2009).

496 (B) BC-box motif from alignment in A. Numbers indicate position in Vif sequence.

497

498 **Figure S2. Affinity Tag Terminus Affects Cullin Specificity of Non-Primate**
499 **Lentiviral Vif Proteins. Related to Figure 1.**

500 (A) Heatmap of analyzed data from Vif AP-MS experiments in HEK293T and
501 Jurkat T-cell lines. AP-MS experiments were scored using the SAINT algorithm
502 using at least 2 experiments per Vif protein per cell line, comparing Vif results to

503 controls. HEK293T data and Jurkat data were scored separately. Interactors are
504 colored by SAINT score and clustered hierarchically by correlation.

505 (B) SDS-PAGE immunoblot of a Flag affinity purification of Flag-tagged Vif
506 proteins induced from stable Jurkat TRex cells, probing for CRL proteins
507 highlighted in **Figure 1D**.

508 (C) AP-MS data comparing N-terminus (N) versus C-terminus (C) 2xStrep affinity
509 tagging of Vif proteins. Heatmap denotes SAINT probabilities of interactions.
510 Data from 7-10 replicate AP-MS experiments per terminus in 293T cells.

511 (D) Immunoblotting of affinity purifications from transient transfections of
512 HEK293T cells comparing N-terminus versus C-terminus 2xStrep tagging of Vif
513 proteins.

514

515 **Figure S3. HIV-1 and MVV Vif-ELOB-ELOC trimers are stabilized by**
516 **cofactors, and additional CYPA residues perturbed in presence of the MVV**
517 **Vif peptide. Related to Figure 4.**

518 (A) UV absorbance curves for recombinantly expressed and purified HIV-1 Vif-
519 ELOB-ELOC complex with and without CBFβ. Samples fractionated by size-
520 exclusion chromatography.

521 (B) UV absorbance curves for recombinantly expressed and purified MVV Vif-
522 ELOB-ELOC complex with and without CYPA. Samples fractionated by size-
523 exclusion chromatography.

524 (C) Different types of perturbations are observed on CYPA HSQC spectrum upon
525 addition of the MVV Vif peptide: peaks disappear (orange sticks, see also **Figure**
526 **4C**), broaden (pink sticks) or enter slow exchange (yellow sticks). All the residues
527 affected are located in or around the active site of CYPA.

528

529 **Figure S4. Blocking CYPA Interactions affects MVV Vif activity but does not**
530 **affect non-interacting HIV-1 Vif activity. Related to Figures 4, 6.**

531 (A) Strep affinity purification of MVV Vif-2xStrep, CAEV Vif-2xStrep, and HIV-1
532 Vif-2xStrep. Co-purification of CYPA is assayed by immunoblotting.

533 (B) Strep affinity purification of Strep tagged HIV-1 Capsid (CA) in the presence
534 of a titration of CsA. Co-purification of CYPA is assayed by immunoblotting. E:
535 ethanol.

536 (C) Strep affinity purification of MVV Vif-2xStrep, MVV Capsid-2xStrep, and HIV-1
537 Capsid-2xStrep. Co-purification of CYPA is assayed by immunoblotting. CA:
538 Capsid.

539 (D) MVV Vif-mediated degradation of OaA3Z2Z3 in the presence of a titration of
540 CsA in HEK293T cells. A3 stability is assayed by Western blot. Bars represent
541 HA immunoreactivity normalized first by GAPDH loading control, then to no Vif
542 control, mean \pm S.D. (n=3). E: ethanol.

543 (E) Assay in **B** performed with HIV-1 Vif and HsA3G.

544 (F) Comparison of HIV-1 Vif HsA3G degradation activity in monoclonal CYPA
545 knockdown versus control cells in the presence or absence of CsA. Bars

546 represent HA immunoreactivity normalized first by GAPDH loading control, then
547 to no Vif control for each cell line; mean \pm S.E. (n=3). Control for assay in **Figure**
548 **6A.**

549

550 **Figure S5. SAXS analysis of reconstituted MVV Vif-CYPA-CRL5 and HIV-1**
551 **Vif¹⁻¹⁷⁴-CBFβ-CRL5. Related to Figure 4.**

552 (A-B) SAXS experimental scattering profiles for **A** HIV-1 E3 and **B** MVV E3. The
553 upper inset shows the SAXS profiles in the Guinier plot with an radius of gyration
554 (Rg) fit of 55.7 ± 0.4 Å and 60.1 ± 0.1 Å for the HIV-1 E3 and MVV E3,
555 respectively.

556 (C) A Kratky plot (q vs. q²I(q)) of the scattering curve indicates the complexes
557 were all folded. The HIV-1 E3 is shown in blue, and the MVV E3 is shown in red.

558 (D) AllosMod FoXS server was used to refine the HIV-1 E3 model to the
559 experimental SAXS profile. The top plot is of the experimental scattering curve
560 and the red curve is the theoretical scattering profile calculated from the atomic
561 resolution HIV-1 E3 model inset into the plot. The model fits the experimental
562 scattering profile with a $\chi = 1.89$. The lower plot shows the residuals (calculated
563 intensity / experimental intensity) of each calculated SAXS profile.

564

565 **Figure S6. MVV Vif mutants result in A3-mediated restriction in primary**
566 **sheep cells. Related to Figure 5.**

567 (A-C) Per-genome context of G-to-A mutations observed in proviral genomes
568 with various MVV Vif mutants.
569 (D) Tri-nucleotide context of observed G-to-A mutations from MVV hypermutation
570 assay in **Figure 5C**, summarized in **Figure 5D**.
571 (E) MVV spreading assay performed in SCP cells with various Vif mutants,
572 identical to the experimental setup in **Figure 5E**.

573

574 **Figure S7. Active-site CYPA mutants fail to rescue MVV Vif function but**
575 **still interact physically. Related to Figure 6.**

576 (A) Model of CYPA showing residues R55, F113, and H126. PDB: 1CWA
577 (B) Monoclonal knockdown line of CYPA is transfected with HA tagged
578 OaA3Z2Z3, Strep-tagged MVV Vif, and various constructs of Flag-tagged CYPA.
579 Vif activity is assessed by OaA3Z2Z3 stability. HA immunoreactivity is
580 normalized by GAPDH signal and to lane 2 control; mean \pm S.E. (n=2).
581 (C) UV absorbance curves for recombinantly expressed and purified MVV-ELOB-
582 ELOC complex with either R55K, F113W, or H126A CYPA. Samples fractionated
583 by size-exclusion chromatography.
584 (D) Coomassie-stained SDS-PAGE of peak fractions from C.

585

586 **SUPPLEMENTAL TABLES**

587 **Table S1**

588

Lentivirus	Strain	Host	Primary Cell Tropism	Disease	Vif Length (a.a.'s)	No. of Host APOBEC3 (Degraded by Vif)
Maedi-Visna Virus (MVV)	Iceland	<i>Ovis aries</i>	Monocytes/ Macrophages ^a	Dyspnea, Paraplegia ^a	230	4 (2) ^{g,h}
Bovine Immunodeficiency Virus (BIV)	p127	<i>Bos taurus</i>	Monocytes/ Macrophages ^b	Lymphocytosis, emaciation, CNS lesions ^b	198	4 (2) ^{g,h}
Feline Immunodeficiency Virus (FIV)	NCSU	<i>Felis sp.</i>	T Lymphocytes ^c	AIDS ^c	251	5 (2) ^{h,i}
Simian Immunodeficiency Virus (SIV)	mac239	<i>Macaca mulatta</i>	T Lymphocytes ^d	AIDS ⁴	214	7 (5) ^{h,j}
Human Immunodeficiency Virus 1 (HIV-1)	NL4-3	<i>Homo sapiens</i>	T Lymphocytes ^{e,f}	AIDS ^{e,f}	192	7 (5) ^{j,k}

589

590 **Table S3**

591

	Rg, from Guinier (Å)	Rg, from P(r) (Å)	Dmax (Å)
HIV-1 E3	55.70	56.94	190
MVV E3	59.37	61.47	200

592

593 **SUPPLEMENTAL TABLE LEGENDS**

594

595 **Table S1. Description of lentiviruses examined in this study. Related to**596 **Figure 1.**

597 a. (Torsteinsdottir et al., 2007), b. (St-Louis et al., 2004), c. (Ackley et al., 1990),

598 d. (Letvin et al., 1985), e. (Barré-Sinoussi et al., 1983), f. (Gallo et al., 1983), g.

599 (Jónsson et al., 2006), h. (LaRue et al., 2008), i. (Münk et al., 2008), j. (Hultquist
600 et al., 2011), k. (Jarmuz et al., 2002)

601

602 **Table S2. SAINT Scored Mass Spectrometry Data. Related to Figure 1.**

603 Data for heatmap shown in **Figure S2A**. SAINT (Choi et al., 2011) probability
604 scores for affinity purification – mass spectrometry (AP-MS) experiments using
605 Vif baits. SAINT probabilities are measured from 0 (no interaction) to 1 (very
606 likely interaction). Scores for each cell line (293T, Jurkat) are listed separately
607 and noted in the column name next to the Vif protein (e.g. SIVmac Vif HEK293T).
608 Scores are shown for identified prey proteins where at least one Vif had a SAINT
609 interaction score ≥ 0.9 in at least one cell line.

610

611 **Table S3. Supplemental SAXS Envelope Data. Related to Figure 4.**

612 Second and third columns indicate the radius of gyration (R_g) calculated from
613 Guinier plot and pair distance distribution function $P(r)$, respectively. The fourth
614 column indicates the maximum distance in $P(r)$, D_{max} .

615

616 **SUPPLEMENTAL REFERENCES**

617

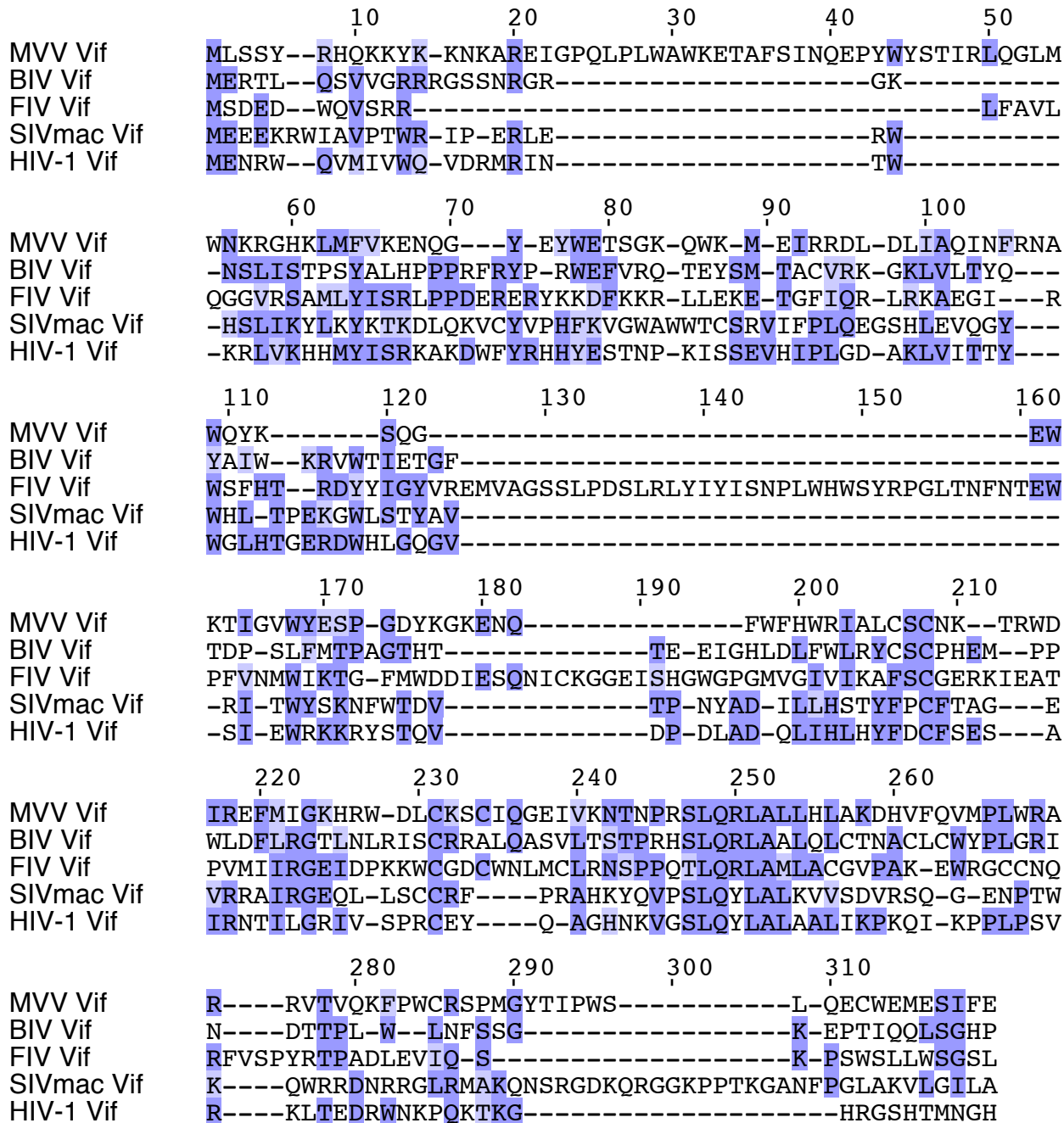
- 618 Ackley, C.D., Yamamoto, J.K., Levy, N., Pedersen, N.C., and Cooper, M.D.
619 (1990). Immunologic abnormalities in pathogen-free cats experimentally infected
620 with feline immunodeficiency virus. *J. Virol.* *64*, 5652–5655.
- 621 Barré-Sinoussi, F., Chermann, J.C., Rey, F., Nugeyre, M.T., Chamaret, S.,
622 Gruest, J., Dauguet, C., Axler-Blin, C., Vézinet-Brun, F., Rouzioux, C., et al.

- 623 (1983). Isolation of a T-lymphotropic retrovirus from a patient at risk for acquired
624 immune deficiency syndrome (AIDS). *Science* *220*, 868–871.
- 625 Castresana, J. (2000). Selection of conserved blocks from multiple alignments for
626 their use in phylogenetic analysis. *Mol. Biol. Evol.* *17*, 540–552.
- 627 Choi, H., Larsen, B., Lin, Z.-Y., Breitkreutz, A., Mellacheruvu, D., Fermin, D., Qin,
628 Z.S., Tyers, M., Gingras, A.-C., and Nesvizhskii, A.I. (2011). SAINT: probabilistic
629 scoring of affinity purification-mass spectrometry data. *Nat. Methods* *8*, 70–73.
- 630 Dereeper, A., Guignon, V., Blanc, G., Audic, S., Buffet, S., Chevenet, F.,
631 Dufayard, J.-F., Guindon, S., Lefort, V., Lescot, M., et al. (2008). Phylogeny.fr:
632 robust phylogenetic analysis for the non-specialist. *Nucleic Acids Res.* *36*,
633 W465–W469.
- 634 Franke, D., and Svergun, D.I. (2009). DAMMIF , a program for rapid ab-initio
635 shape determination in small-angle scattering. *J. Appl. Crystallogr.* *42*, 342–346.
- 636 Gallo, R.C., Sarin, P.S., Gelmann, E.P., Robert-Guroff, M., Richardson, E.,
637 Kalyanaraman, V.S., Mann, D., Sidhu, G.D., Stahl, R.E., Zolla-Pazner, S., et al.
638 (1983). Isolation of human T-cell leukemia virus in acquired immune deficiency
639 syndrome (AIDS). *Science* *220*, 865–867.
- 640 Haché, G., Shindo, K., Albin, J.S., and Harris, R.S. (2008). Evolution of HIV-1
641 Isolates that Use a Novel Vif-Independent Mechanism to Resist Restriction by
642 Human APOBEC3G. *Curr. Biol.* *18*, 819–824.
- 643 De Hoon, M.J.L., Imoto, S., Nolan, J., and Miyano, S. (2004). Open source
644 clustering software. *Bioinformatics* *20*, 1453–1454.
- 645 Hultquist, J.F., Lengyel, J.A., Refsland, E.W., LaRue, R.S., Lackey, L., Brown,
646 W.L., Harris, R.S., and Apobec3, R. (2011). Human and rhesus APOBEC3D,
647 APOBEC3F, APOBEC3G, and APOBEC3H demonstrate a conserved capacity to
648 restrict Vif-deficient HIV-1. *J. Virol.* *85*, 11220–11234.
- 649 Jäger, S., Cimermancic, P., Gulbahce, N., Johnson, J.R., McGovern, K.E.,
650 Clarke, S.C., Shales, M., Mercenne, G., Pache, L., Li, K., et al. (2012a). Global
651 landscape of HIV-human protein complexes. *Nature* *481*, 365–370.
- 652 Jäger, S., Kim, D.Y., Hultquist, J.F., Shindo, K., LaRue, R.S., Kwon, E., Li, M.,
653 Anderson, B.D., Yen, L., Stanley, D., et al. (2012b). Vif hijacks CBF-β to degrade
654 APOBEC3G and promote HIV-1 infection. *Nature* *481*, 371–375.

- 655 Jarmuz, A., Chester, A., Bayliss, J., Gisbourne, J., Dunham, I., Scott, J., and
656 Navaratnam, N. (2002). An anthropoid-specific locus of orphan C to U RNA-
657 editing enzymes on chromosome 22. *Genomics* **79**, 285–296.
- 658 Jónsson, S.R., Haché, G., Stenglein, M.D., Fahrenkrug, S.C., Andrésdóttir, V.,
659 and Harris, R.S. (2006). Evolutionarily conserved and non-conserved retrovirus
660 restriction activities of artiodactyl APOBEC3F proteins. *Nucleic Acids Res.* **34**,
661 5683–5694.
- 662 Kingston, R.E., Chen, C.A., and Okayama, H. (2003). Calcium phosphate
663 transfection. *Curr. Protoc. Cell Biol. Chapter 20*, Unit 20.3.
- 664 Konarev, P. V., Petoukhov, M. V., Volkov, V. V., and Svergun, D.I. (2006).
665 ATSAS 2.1, a program package for small-angle scattering data analysis. *J. Appl.*
666 *Crystallogr.* **39**, 277–286.
- 667 LaRue, R.S., Jónsson, S.R., Silverstein, K.A.T., Lajoie, M., Bertrand, D., El-
668 Mabrouk, N., Hötzl, I., Andrésdóttir, V., Smith, T.P.L., and Harris, R.S. (2008).
669 The artiodactyl APOBEC3 innate immune repertoire shows evidence for a multi-
670 functional domain organization that existed in the ancestor of placental
671 mammals. *BMC Mol. Biol.* **9**, 104.
- 672 LaRue, R.S., Lengyel, J., Jónsson, S.R., Andrésdóttir, V., and Harris, R.S.
673 (2010). Lentiviral Vif degrades the APOBEC3Z3/APOBEC3H protein of its
674 mammalian host and is capable of cross-species activity. *J. Virol.* **84**, 8193–
675 8201.
- 676 Letvin, N.L., Daniel, M.D., Sehgal, P.K., Desrosiers, R.C., Hunt, R.D., Waldron,
677 L.M., MacKey, J.J., Schmidt, D.K., Chalifoux, L. V, and King, N.W. (1985).
678 Induction of AIDS-like disease in macaque monkeys with T-cell tropic retrovirus
679 STLV-III. *Science* **230**, 71–73.
- 680 Li, M., Shandilya, S.M.D., Carpenter, M.A., Rathore, A., Brown, W.L., Perkins,
681 A.L., Harki, D.A., Solberg, J., Hook, D.J., Pandey, K.K., et al. (2012). First-in-
682 class small molecule inhibitors of the single-strand DNA cytosine deaminase
683 APOBEC3G. *ACS Chem. Biol.* **7**, 506–517.
- 684 Münk, C., Beck, T., Zielonka, J., Hotz-Wagenblatt, A., Chareza, S., Battenberg,
685 M., Thielebein, J., Cichutek, K., Bravo, I.G., O'Brien, S.J., et al. (2008).
686 Functions, structure, and read-through alternative splicing of feline APOBEC3
687 genes. *Genome Biol.* **9**, R48.
- 688 Notredame, C., Higgins, D.G., and Heringa, J. (2000). T-Coffee: A novel method
689 for fast and accurate multiple sequence alignment. *J. Mol. Biol.* **302**, 205–217.

- 690 Nowarski, R., Britan-Rosich, E., Shiloach, T., and Kotler, M. (2008).
691 Hypermutation by intersegmental transfer of APOBEC3G cytidine deaminase.
692 *Nat. Struct. Mol. Biol.* *15*, 1059–1066.
- 693 Pettersen, E.F., Goddard, T.D., Huang, C.C., Couch, G.S., Greenblatt, D.M.,
694 Meng, E.C., and Ferrin, T.E. (2004). UCSF Chimera--a visualization system for
695 exploratory research and analysis. *J. Comput. Chem.* *25*, 1605–1612.
- 696 R Core Team (2014). R: A Language and Environment for Statistical Computing.
- 697 Rasband, W.S. (2007). ImageJ.
- 698 Rice, P., Longden, I., and Bleasby, A. (2000). EMBOSS: the European Molecular
699 Biology Open Software Suite. *Trends Genet.* *16*, 276–277.
- 700 Saldanha, A.J. (2004). Java Treeview--extensible visualization of microarray
701 data. *Bioinformatics* *20*, 3246–3248.
- 702 Sali, A., and Blundell, T.L. (1993). Comparative protein modelling by satisfaction
703 of spatial restraints. *J. Mol. Biol.* *234*, 779–815.
- 704 Schneidman-Duhovny, D., Hammel, M., and Sali, A. (2010). FoXS: a web server
705 for rapid computation and fitting of SAXS profiles. *Nucleic Acids Res.* *38*, W540–
706 W544.
- 707 St-Louis, M.-C., Cojocariu, M., and Archambault, D. (2004). The molecular
708 biology of bovine immunodeficiency virus: a comparison with other lentiviruses.
709 *Anim. Health Res. Rev.* *5*, 125–143.
- 710 Stamatakis, A., Hoover, P., and Rougemont, J. (2008). A rapid bootstrap
711 algorithm for the RAxML Web servers. *Syst. Biol.* *57*, 758–771.
- 712 Stanley, D.J., Bartholomeeusen, K., Crosby, D.C., Kim, D.Y., Kwon, E., Yen, L.,
713 Cartozo, N.C., Li, M., Jäger, S., Mason-Herr, J., et al. (2012). Inhibition of a
714 NEDD8 Cascade Restores Restriction of HIV by APOBEC3G. *PLoS Pathog.* *8*,
715 e1003085.
- 716 Stenglein, M.D., and Harris, R.S. (2006). APOBEC3B and APOBEC3F inhibit L1
717 retrotransposition by a DNA deamination-independent mechanism. *J. Biol. Chem.*
718 *281*, 16837–16841.
- 719 Stenglein, M.D., Burns, M.B., Li, M., Lengyel, J., and Harris, R.S. (2010).
720 APOBEC3 proteins mediate the clearance of foreign DNA from human cells. *Nat.*
721 *Struct. Mol. Biol.* *17*, 222–229.

- 722 Svergun, D.I. (1999). Restoring low resolution structure of biological
723 macromolecules from solution scattering using simulated annealing. *Biophys. J.*
724 *76*, 2879–2886.
- 725 Torsteinsdottir, S., Andresdottir, V., Arnarson, H., and Petursson, G. (2007).
726 Immune response to maedi-visna virus. *Front. Biosci.* *12*, 1532–1543.
- 727 Volkov, V. V., and Svergun, D.I. (2003). Uniqueness of ab initio shape
728 determination in small-angle scattering. *J. Appl. Crystallogr.* *36*, 860–864.
- 729 Vranken, W.F., Boucher, W., Stevens, T.J., Fogh, R.H., Pajon, A., Llinas, M.,
730 Ulrich, E.L., Markley, J.L., Ionides, J., and Laue, E.D. (2005). The CCPN data
731 model for NMR spectroscopy: development of a software pipeline. *Proteins* *59*,
732 687–696.
- 733 Waterhouse, A.M., Procter, J.B., Martin, D.M. a, Clamp, M., and Barton, G.J.
734 (2009). Jalview Version 2--a multiple sequence alignment editor and analysis
735 workbench. *Bioinformatics* *25*, 1189–1191.
- 736 Weinkam, P., Pons, J., and Sali, A. (2012). Structure-based model of allostery
737 predicts coupling between distant sites. *Proc. Natl. Acad. Sci. U. S. A.* *109*,
738 4875–4880.
- 739

A**B**

MVV Vif	173 - SLQRLALLHL - 182
BIV Vif	150 - SLQRLAALQL - 159
FIV Vif	200 - TLQRLAMLAC - 209
SIVmac Vif	147 - SLQYLALKVV - 156
HIV-1 Vif	144 - SLQYLALALA - 153

BC-Box

Figure S1

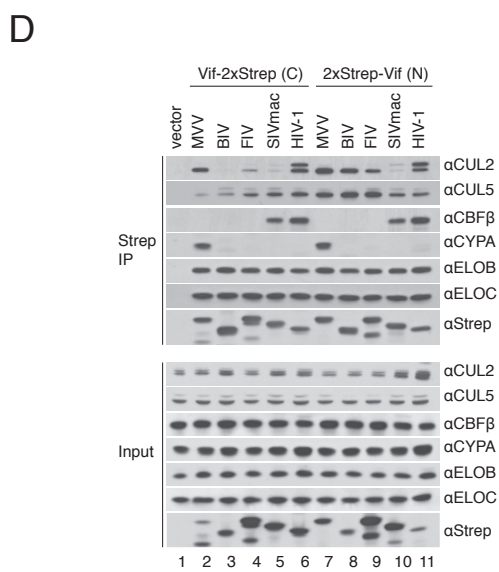
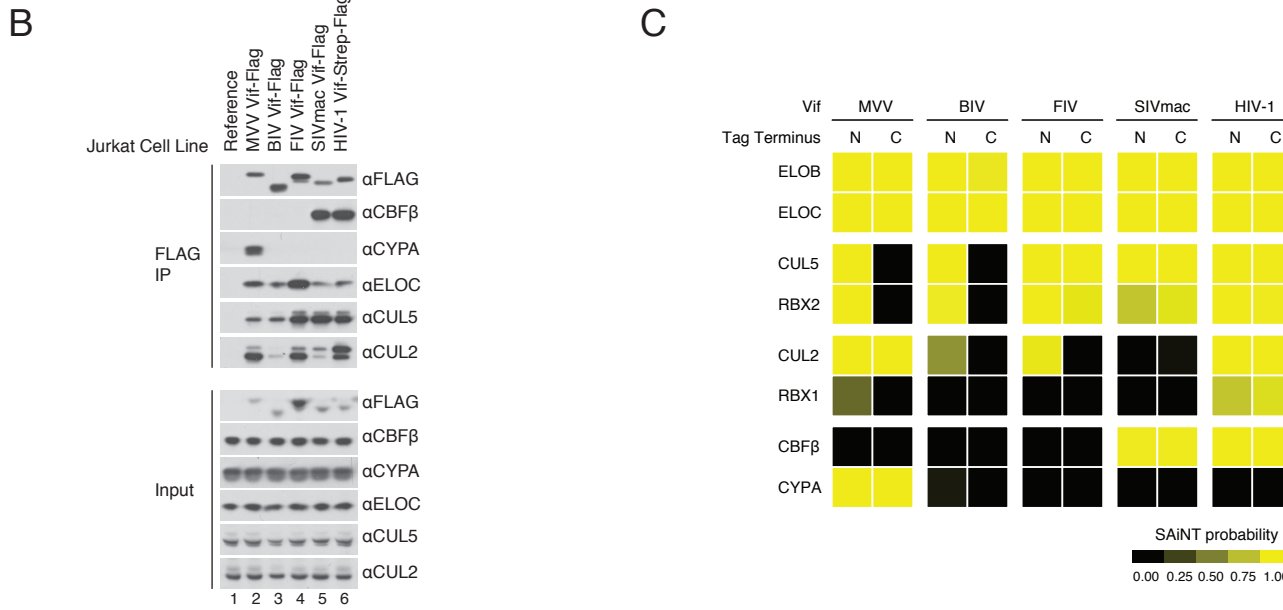
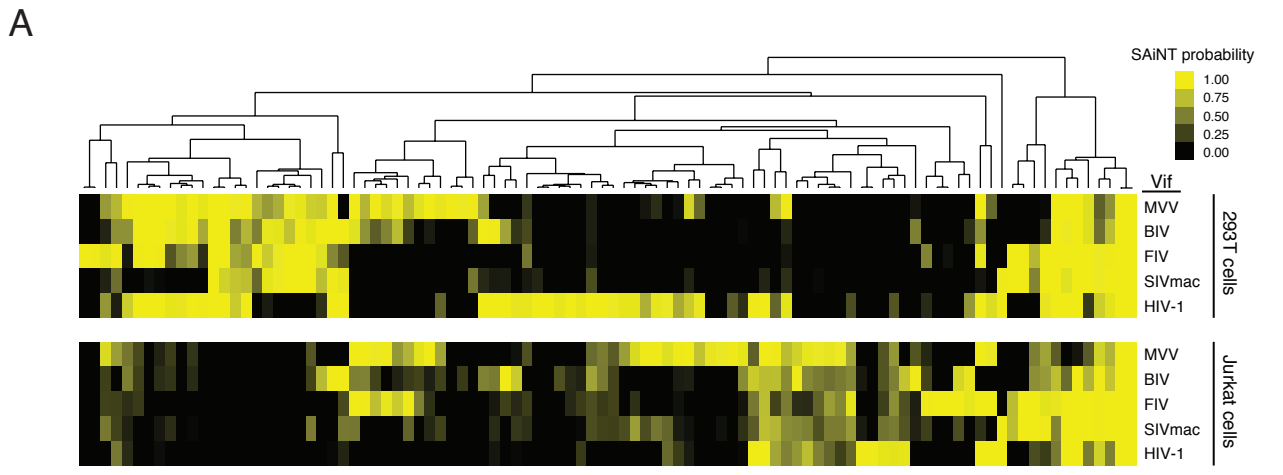


Figure S2

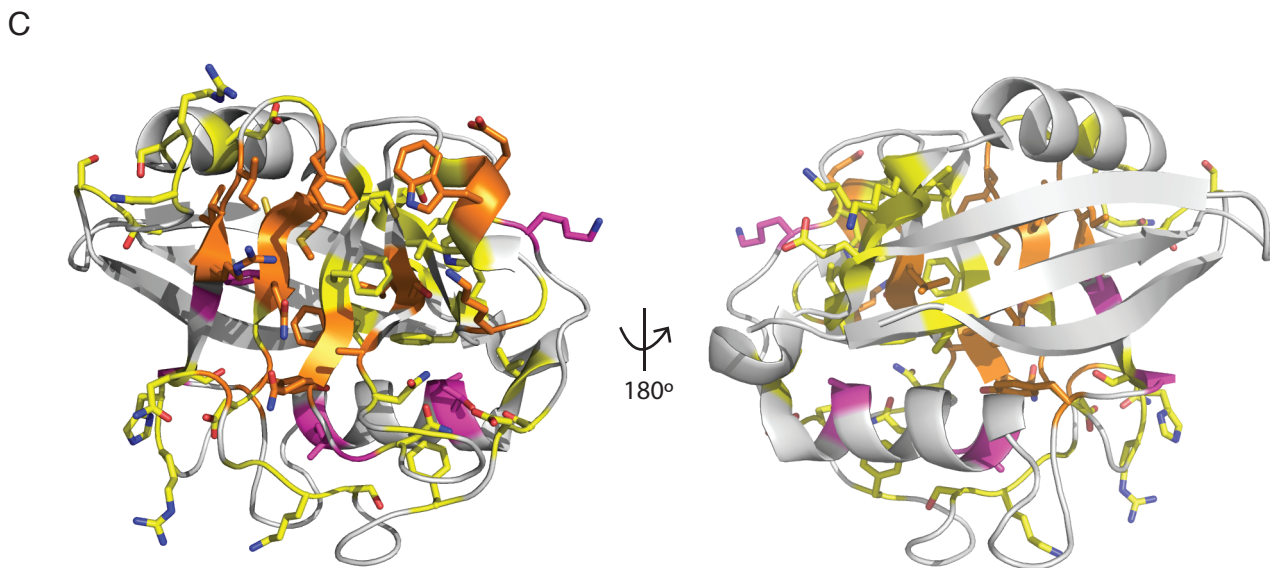
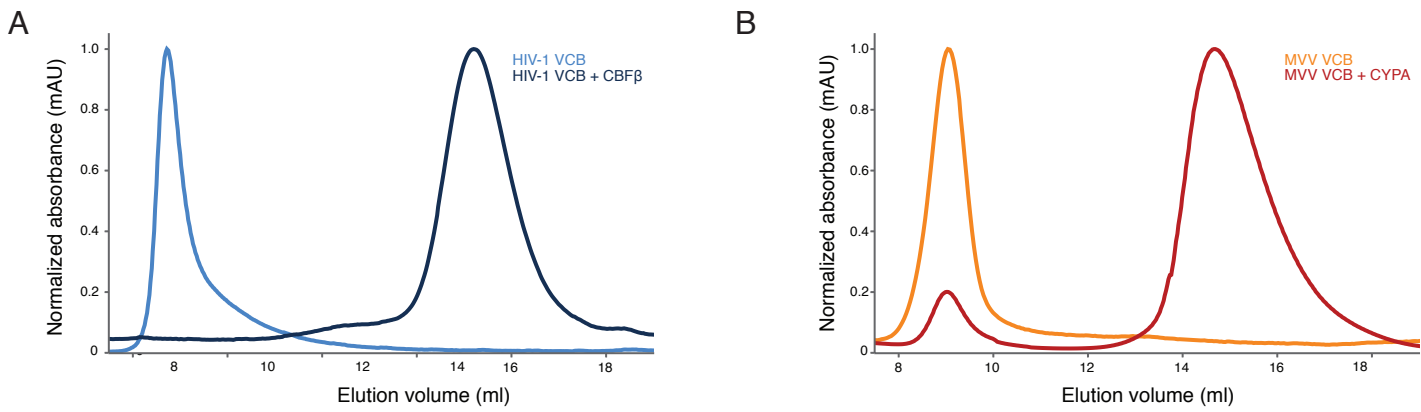
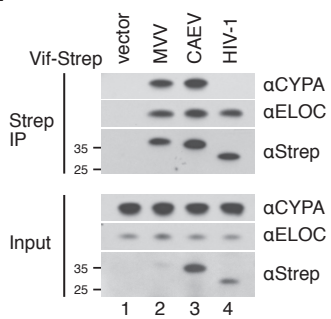
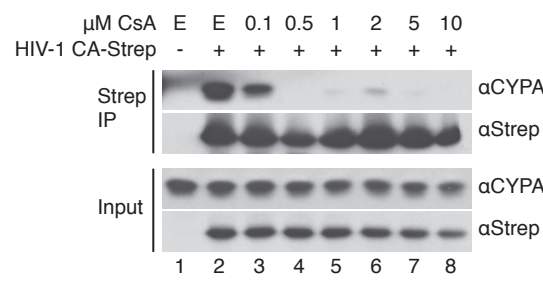


Figure S3

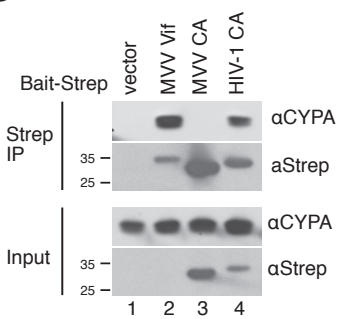
A



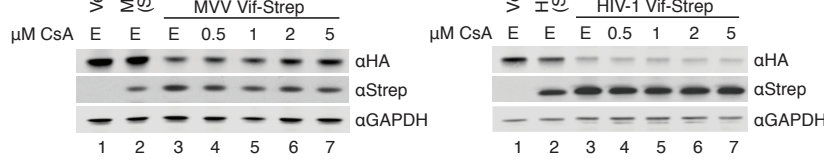
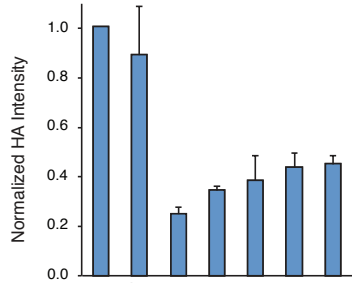
B



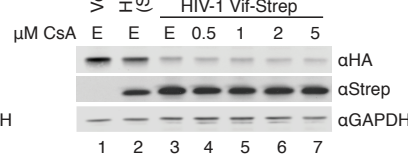
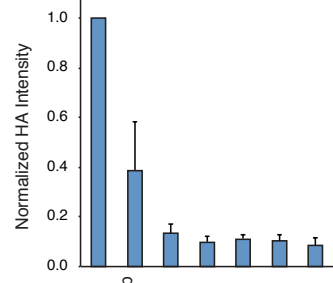
C



D



E



F

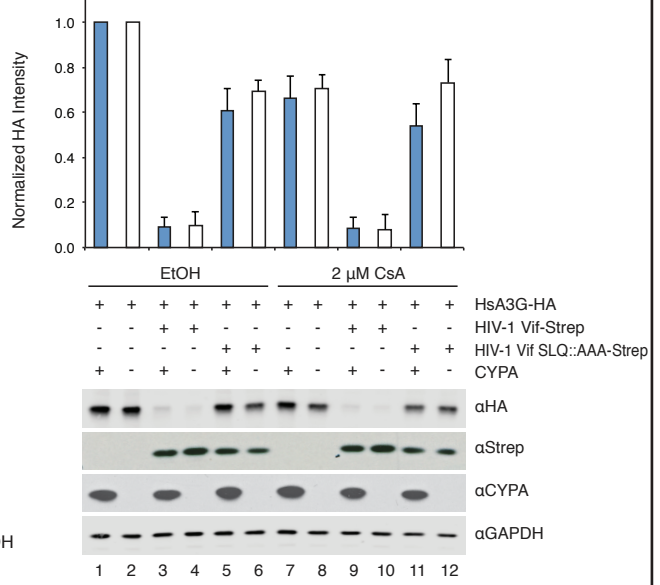


Figure S4

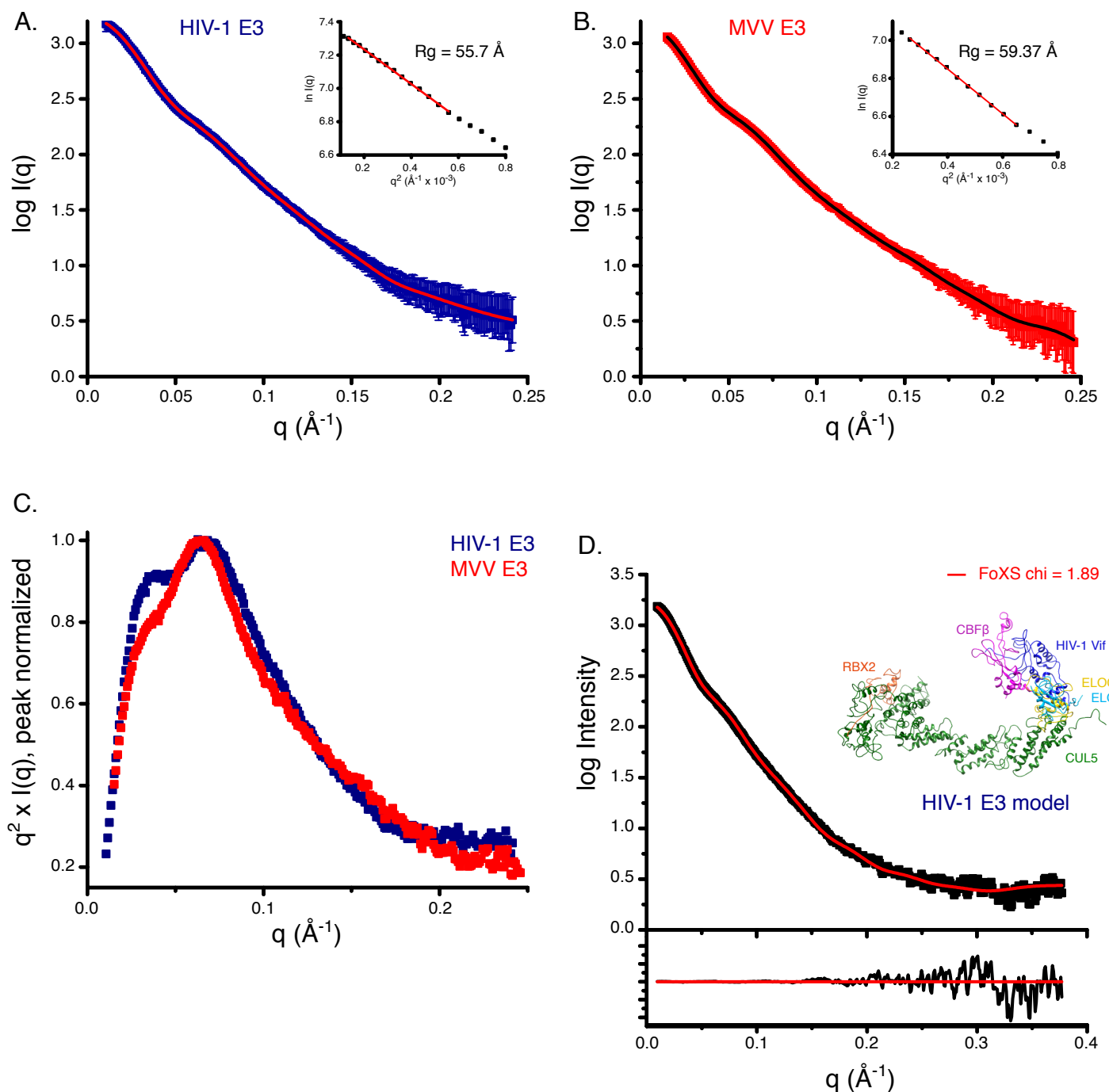
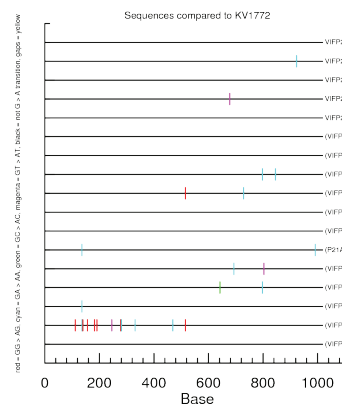


Figure S5

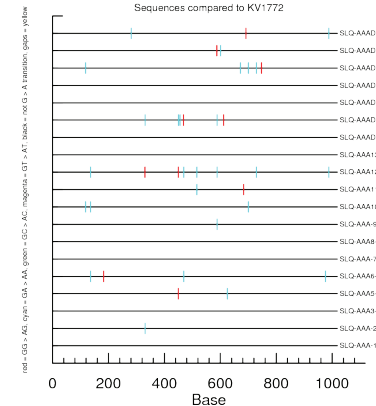


P21A/P24A



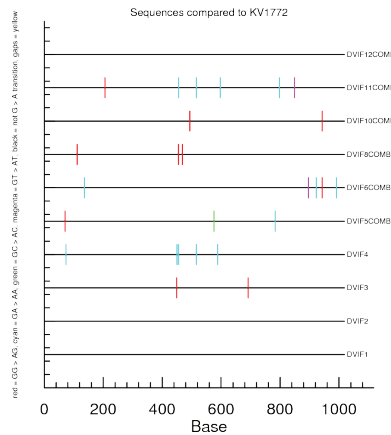
B

SLQ::AAA

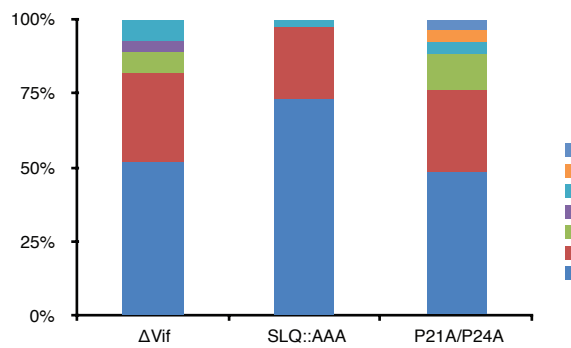


C

ΔV_{if}



D



█	GAT
█	GCT
█	GGG
█	GCA
█	GTA
█	GGA
█	GAA

E

Vif

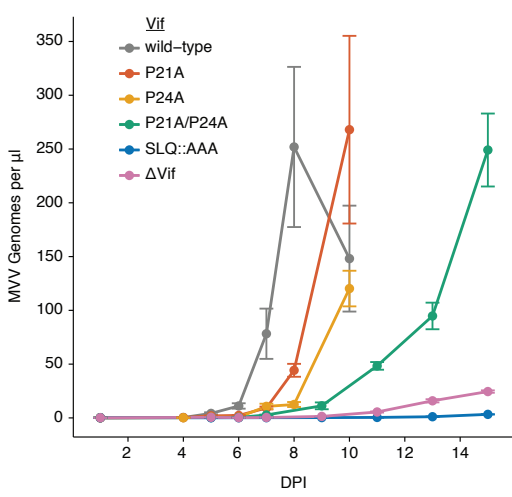
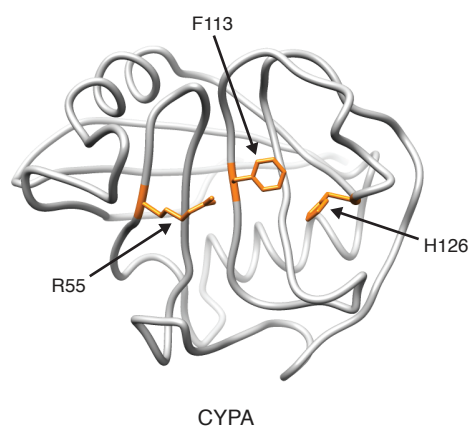
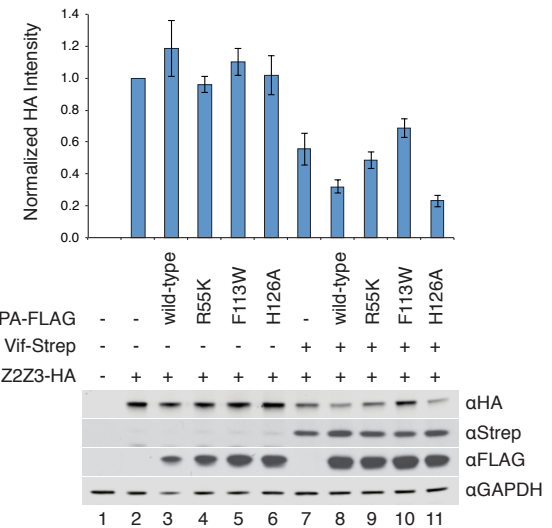
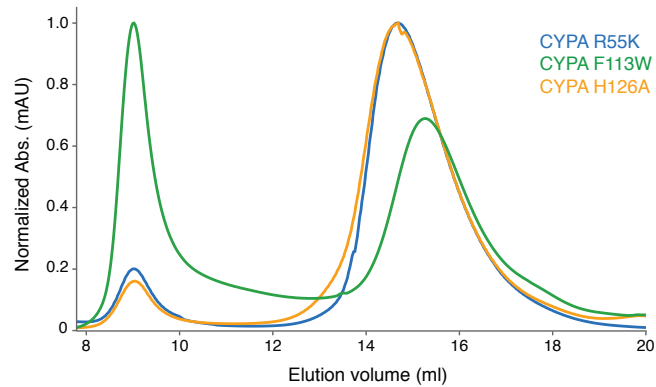
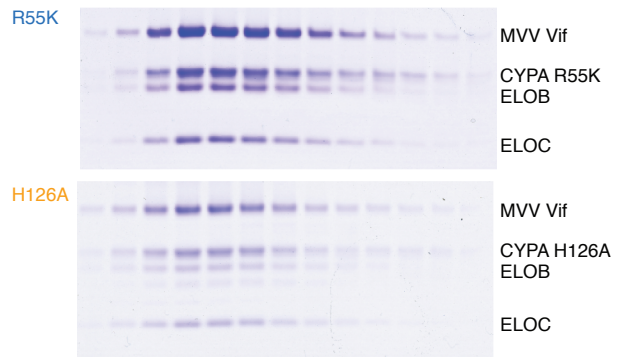


Figure S6

A**B****C****D****Figure S7**